KIM-1–mediated phagocytosis reduces acute injury to the kidney

Li Yang,[1,2] Craig R. Brooks,[1] Sheng Xiao,[3] Venkata Sabbisetti,[1] Melissa Y. Yeung,[1,4] Li-Li Hsiao,[1] Takaharu Ichimura,[1] Vijay Kuchroo,[3] and Joseph V. Bonventre[1,5]

[1]Renal Division, Brigham and Women's Hospital, Department of Medicine, Harvard Medical School, Boston, Massachusetts, USA. [2]Renal Division, Department of Medicine, Peking University First Hospital, Peking University Institute of Nephrology, Key Laboratory of Renal Disease, Ministry of Health of China, Beijing, China. [3]Center for Neurologic Disease, Brigham and Women's Hospital, Harvard Medical School, Boston, Massachusetts, USA. [4]Transplantation Research Center, Renal Division, Brigham and Women's Hospital, Harvard Medical School, Boston, Massachusetts, USA. [5]Harvard Stem Cell Institute, Cambridge, Massachusetts, USA.

Kidney injury molecule 1 (KIM-1, also known as TIM-1) is markedly upregulated in the proximal tubule after injury and is maladaptive when chronically expressed. Here, we determined that early in the injury process, however, KIM-1 expression is antiinflammatory due to its mediation of phagocytic processes in tubule cells. Using various models of acute kidney injury (AKI) and mice expressing mutant forms of KIM-1, we demonstrated a mucin domain–dependent protective effect of epithelial KIM-1 expression that involves downregulation of innate immunity. Deletion of the mucin domain markedly impaired KIM-1–mediated phagocytic function, resulting in increased proinflammatory cytokine production, decreased antiinflammatory growth factor secretion by proximal epithelial cells, and a subsequent increase in tissue macrophages. Mice expressing KIM-1$^{\Delta mucin}$ had greater functional impairment, inflammatory responses, and mortality in response to ischemia- and cisplatin-induced AKI. Compared with primary renal proximal tubule cells isolated from KIM-1$^{\Delta mucin}$ mice, those from WT mice had reduced proinflammatory cytokine secretion and impaired macrophage activation. The antiinflammatory effect of KIM-1 expression was due to the interaction of KIM-1 with p85 and subsequent PI3K-dependent downmodulation of NF-κB. Hence, KIM-1–mediated epithelial cell phagocytosis of apoptotic cells protects the kidney after acute injury by downregulating innate immunity and inflammation.

Introduction

Acute kidney injury (AKI) is a very common clinical condition. The incidence of hospital-acquired AKI is increasing, and many patients require renal replacement therapy (1, 2). Severe AKI is associated with in-hospital mortality rates of greater than 60% (2). There are also chronic consequences, even if the patients survive their acute illness. Whether or not patients have preexisting chronic kidney disease (CKD), those who have had AKI have a high risk of developing progressive CKD and end-stage renal disease (ESRD) over time (3–5).

In contrast to the heart or brain, the kidney can effectively recover from an ischemic or toxic insult that results in cell death, since the tubular epithelium has a potent ability to proliferate and replace lost cells (6–8). This repair, however, can also be maladaptive, leading to CKD or its progression if the injury is severe or repeated or occurs in the setting of CKD (9, 10). The balance between injury and repair is the key determinant of the fate of the injured kidney, and one might expect that there are potent factors induced by injury to facilitate adaptive repair. AKI results in inflammation, which exacerbates tubular injury (11). Control of the inflammation is important to minimize injury and facilitate recovery from kidney injury. The focus of proposed therapies has, to date, been primarily directed at proinflammatory factors, and less attention has been paid to the understanding of the endogenous factors normally involved in the downregulation of inflammation.

Many studies have demonstrated that the tubular epithelium is not merely a passive victim of injury. Tubular epithelial cells generate important proinflammatory cytokines and chemokines and express TLRs, making them an important component of the innate immune response. Kidney injury molecule 1/T cell Ig and mucin domain 1 (KIM-1/TIM-1) is upregulated more than any other protein in the proximal tubule of the kidney, with various forms of injury (12, 13). KIM-1 is a phosphatidylserine receptor that mediates phagocytosis of apoptotic bodies and oxidized lipids (14). When KIM-1 is expressed chronically, it results in progressive kidney fibrosis and chronic kidney failure (15), which is perhaps related to its phagocytic function to take up noxious compounds, such as oxidized lipids. In addition to its role in phagocytosis, KIM-1 can activate signaling through the PI3 kinase pathway (16). The role of KIM-1 signaling in proximal tubular cells (PTCs), as well as the connection between KIM-1 phagocytosis and phosphorylation, has yet to be determined. Here, we characterize a KIM-1–mutant mouse that is deficient in phagocytosis, phosphorylation, and interaction with p85. We demonstrate for the first time, to our knowledge, that KIM-1–mediated phagocytic

Authorship note: Li Yang and Craig R. Brooks are co–first authors and contributed equally to this work.

Conflict of interest: Joseph V. Bonventre is a coinventor on KIM-1 patents that are assigned to Partners HealthCare and licensed by Partners HealthCare to Johnson & Johnson, Sekisui Chemical Company, Biogen Idec, Astute Medical, and a number of research reagent companies.

Submitted: December 15, 2014; **Accepted:** January 22, 2015.

Reference information: *J Clin Invest*. 2015;125(4):1620–1636. doi:10.1172/JCI75417.

function downregulates inflammation and the innate immune response in acute ischemic and toxic injury.

Results

Decreased phagocytic function of KIM-1$^{\Delta mucin}$ in PTCs. A KIM-1–mutant mouse was created by replacing exon 3 of the *KIM-1* gene with a *PGK* promoter–driven neomycin-resistance cassette on a C57BL/6 genetic background. This mutant mouse generated KIM-1 proteins with the loss of the mucin domain, encoded by exon 3 (KIM-1$^{\Delta mucin}$) (17). KIM-1$^{\Delta mucin}$ mice were found to have similar mRNA expression levels of the closest of the TIM genes in the *KIM-1* locus (17). We confirmed that other TIMs, TIM-3 and TIM-4, are not differentially regulated in KIM-1$^{\Delta mucin}$ tubular cells at the protein level or in B cells compared with KIM-1 WT cells (data not shown). KIM-1$^{\Delta mucin}$ interaction with TIM-4 is similar to that in WT KIM-1, indicating that while the KIM-1$^{\Delta mucin}$ mutant was deficient in phagocytosis, it retained other KIM-1 functions (17) and did not result in modification of other TIMs tested. To evaluate whether the deletion of the mucin domain in this mouse affects KIM-1 expression and function, we incubated fluorescently tagged apoptotic cells with primary cultured PTCs obtained from WT and KIM-1$^{\Delta mucin}$ mice and LLC-PK1 cell lines transfected with WT KIM-1 or KIM-1$^{\Delta mucin}$. As shown in Figure 1, A and B, after 7 days in culture, PTCs from both WT mice and KIM-1$^{\Delta mucin}$ mice showed strong anti–KIM-1 Ab staining with an Ab directed against the Ig domain of the molecule. The KIM-1$^{\Delta mucin}$ PTCs had markedly decreased phagocytosis of apoptotic cells compared with that in WT PTCs (20.2 ± 5.8% SD vs. 81.3 ± 7.2% of cells containing apoptotic cells, $P < 0.001$). A similar reduction in phagocytosis was observed in LLC-PK1 cells transfected with *KIM-1/TIM-1$^{\Delta mucin}$* when compared with cells transfected with WT *KIM-1* (15.6 ± 5.6% vs. 91.1 ± 10.4%, $P < 0.001$).

To determine the kinetics of KIM-1–mediated apoptotic cell uptake and phagosomal maturation, KIM-1–expressing LLC-PK1 cells were incubated with apoptotic cells labeled with CytoTracker Green and pHrodo (a pH-sensitive dye that increases in fluorescence intensity in low pH environments). KIM-1–expressing cells bound the apoptotic cells within 30 minutes, and acidification of the phagosome occurred between 2 and 6 hours, with approximately 50% of the apoptotic cells positive for the pHrodo dye at 6 hours (Figure 1C). KIM-1 phagocytosis and phagosomal maturation in epithelial cells were found to be slower compared with professional phagocytes, such as macrophages or DCs, in which phagocytosis and phagosomal acidification occur within 2 hours (data not shown). These data indicate that within 6 hours of being phagocytosed, the apoptotic cells are degraded and undetectable by biochemical assays such as TUNEL. In cell outgrowth assays, KIM-1–expressing CHO cells were found to be more motile than were cells not expressing KIM-1 and displayed a scattering phenotype, whereby the cells migrated individually as opposed to migrating in a monolayer pattern, as was seen with the control CHO cells (Figure 1D). Increased motility may enhance the ability of KIM-1 to phagocytose dead cells.

After ischemia/reperfusion (I/R) injury, more apoptotic bodies were detected by TUNEL staining in the renal tubules of KIM-1$^{\Delta mucin}$ animals when compared with those of WT mice 24 and 48 hours after I/R injury (Figure 1E), while KIM-1 expression at the mRNA level was higher in the WT mice after I/R (Figure 1I). The greater number of apoptotic bodies we observed in the KIM-1$^{\Delta mucin}$ mice was consistent with reduced phagocytosis of TUNEL$^+$ apoptotic cells by PTCs expressing the KIM-1$^{\Delta mucin}$ molecule in vivo. Double staining with TUNEL and anti–KIM-1 Abs revealed apoptotic bodies surrounded by KIM-1 in the WT tubules, while no apparent uptake of apoptotic bodies was seen in KIM-1$^{\Delta mucin}$ I/R-injured mouse kidneys (Figure 1F). In order to determine whether KIM-1–mediated phagocytosis contributed to the reduced numbers of apoptotic cells, lysosomal degradation of apoptotic cells was blocked to prevent the elimination of the apoptotic cells by phagocytic cell processing. The vacuolar H^+-ATPase inhibitor bafilomycin A1 (Baf) inhibits lysosomal and phagosomal acidification, preventing the breakdown of phagocytosed materials. I/R kidneys from WT mice treated with Baf showed an approximate 10-fold increase in the number of TUNEL$^+$ cells, while KIM-1$^{\Delta mucin}$ kidneys had only an approximate 2-fold increase in TUNEL$^+$ cells (Figure 1, G and H). Similar results were found with another lysosomal inhibitor, chloroquine (data not shown). We also examined the presence of luminal debris (without Baf). Twenty-four hours after I/R, both the WT and KIM-1$^{\Delta mucin}$ kidneys displayed similar levels of luminal cellular debris (Figure 1, J and K). By 48 hours, we observed a significant reduction in luminal debris in WT, but not KIM-1$^{\Delta mucin}$, kidneys, which continued out to 72 hours. Taken together, these data demonstrate that KIM-1 and KIM-1$^{\Delta mucin}$ kidneys have similar levels of cell death following I/R injury and that WT KIM-1 is responsible for the phagocytic uptake of much of the luminal apoptotic cells and cellular debris in the injured kidney.

Kidney function and animal survival are worse in KIM-1$^{\Delta mucin}$ mice after I/R or cisplatin insult. To evaluate the role of KIM-1 phagocytic function in renal functional impairment, we determined the plasma creatinine levels in KIM-1$^{\Delta mucin}$ and WT mice. As shown in Figure 2A, 24 hours after the I/R insult, KIM-1$^{\Delta mucin}$ mice had a higher creatinine peak than did WT mice (0.99 ± 0.12 mg/dl vs. 0.50 ± 0.08 mg/dl, $P < 0.05$), demonstrating more severe renal dysfunction. Consistent with the more severe renal dysfunction in KIM-1$^{\Delta mucin}$ mice, we found significantly more widespread tubulointerstitial damage when quantitated in kidneys from these animals from day 1 to day 3 after I/R injury compared with WT kidneys (Figure 2B).

We also investigated whether normal phagocytic function of KIM-1 is protective against cisplatin-mediated toxic AKI. KIM-1$^{\Delta mucin}$ mice showed much higher mortality, with 100% death of the animals versus 0% death of the WT mice within 5 days after cisplatin injection (Figure 2C). There was more severe kidney dysfunction in the KIM-1$^{\Delta mucin}$ mice than in WT animals, with KIM-1$^{\Delta mucin}$ mice exhibiting much higher creatinine levels 3 days after cisplatin (Figure 2C). We noted differences in tubulointerstitial damage on day 2. Damage was more widespread on day 4 and was associated with increased inflammatory infiltration in the KIM-1$^{\Delta mucin}$ kidneys (Figure 2, D and E).

PTCs cultured from WT and KIM-1$^{\Delta mucin}$ mice showed similar KIM-1 protein expression levels on various days in culture, as reflected by immunostaining with Abs targeting either extracellular or intracellular KIM-1 domains (Figure 2F). We found no obvious differences in basal proliferative rates between WT and KIM-1$^{\Delta mucin}$ cells, as reflected by equivalent levels of Ki67 staining (Figure 2G).

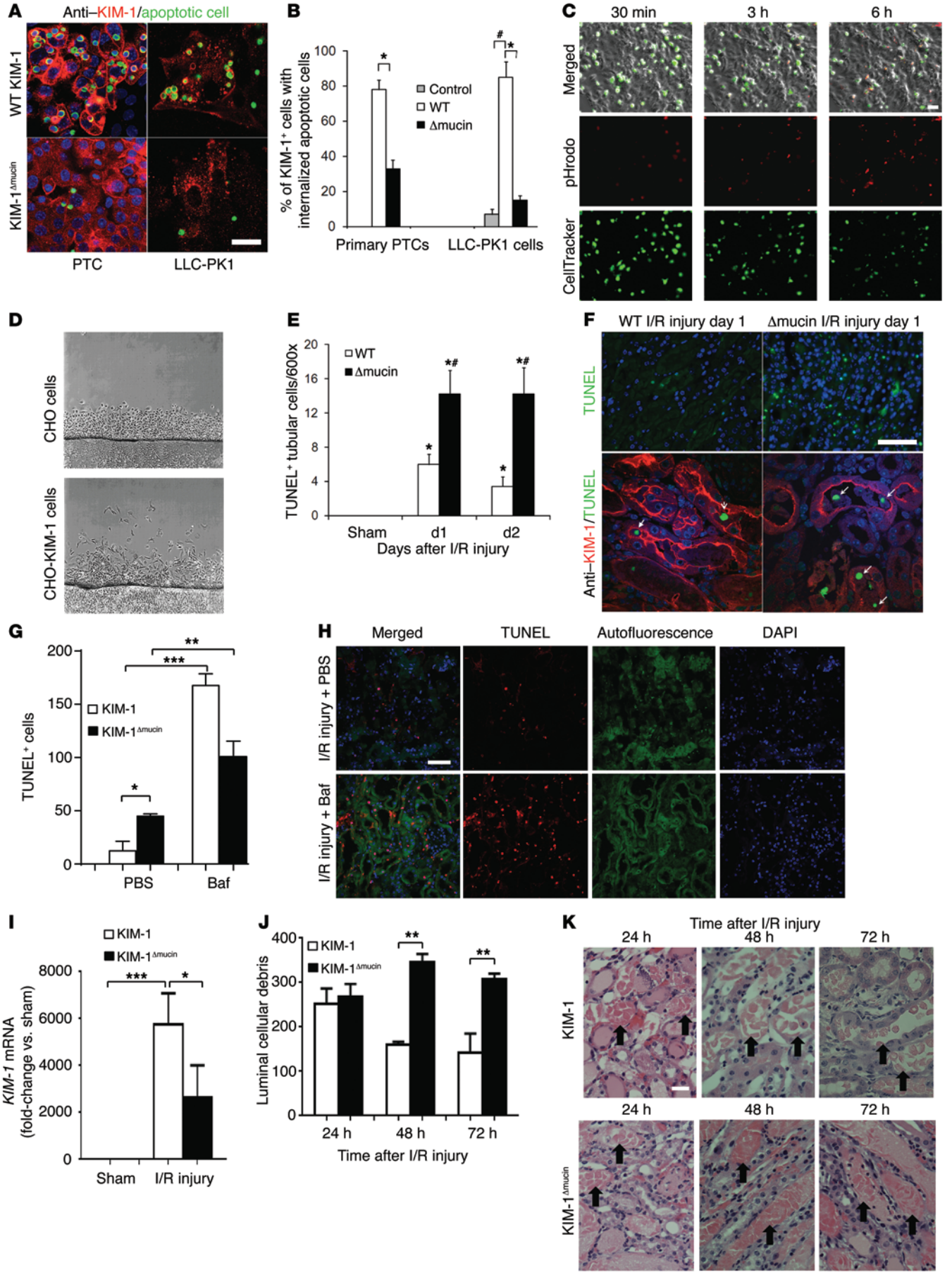
A
Anti–KIM-1/apoptotic cell
WT KIM-1
KIM-1 Δmucin
PTC
LLC-PK1
B
% of KIM-1+ cells with internalized apoptotic cells
Control
WT
Δmucin
Primary PTCs
LLC-PK1 cells
C
30 min
3 h
6 h
Merged
pHrodo
CellTracker
D
CHO cells
CHO-KIM-1 cells
E
TUNEL+ tubular cells/600x
WT
Δmucin
Sham
d1
d2
Days after I/R injury
F
WT I/R injury day 1
Δmucin I/R injury day 1
TUNEL
Anti–KIM-1/TUNEL
G
TUNEL+ cells
KIM-1
KIM-1 Δmucin
PBS
Baf
H
Merged
TUNEL
Autofluorescence
DAPI
I/R injury + PBS
I/R injury + Baf
I
KIM-1 mRNA (fold-change vs. sham)
KIM-1
KIM-1 Δmucin
Sham
I/R injury
J
Luminal cellular debris
KIM-1
KIM-1 Δmucin
24 h
48 h
72 h
Time after I/R injury
K
Time after I/R injury
24 h
48 h
72 h
KIM-1
KIM-1 Δmucin

Figure 1. Decreased phagocytic function of KIM-1$^{\Delta mucin}$ in PTCs. (**A**) Anti–KIM-1 immunostaining (red) in primary PTCs from both WT KIM-1 and KIM-1$^{\Delta mucin}$ mice (left panel) and LLC-PK1 cells transfected with empty vector (control), KIM-1 or KIM-1$^{\Delta mucin}$ (right panel) exposed to apoptotic lymphocytes (green). Scale bar: 20 μm. (**B**) The percentage of PTCs that internalized apoptotic lymphocytes was reduced in the KIM-1$^{\Delta mucin}$ PTCs (n = 3). *P < 0.01; #P < 0.001. (**C**) Representative time course from 5 experiments of the uptake and acidification (red) of apoptotic cells (green) by KIM-1–expressing LLC-PK1 cells. Scale bar: 30 μm. (**D**) Representative images of cell outgrowth from coverslips in CHO cells expressing empty vector or KIM-1 (images are representative of 3 experiments). (**E**) TUNEL$^+$ tubular cells in I/R kidneys from WT KIM-1 and KIM-1$^{\Delta mucin}$ mice (n = 5 mice/time point/group).*P < 0.01 vs. sham; #P < 0.01 vs. WT KIM-1. (**F**) Colocalization of KIM-1 and TUNEL$^+$ cells (arrows in the left panel show KIM-1–binding apoptotic bodies). Scale bar: 50 μm. (**G**) Quantification of TUNEL$^+$ cells in WT KIM-1 and KIM-1$^{\Delta mucin}$ mice 24 hours after I/R injury plus vehicle or I/R injury plus Baf (n = 3). *P < 0.05; **P < 0.01; ***P < 0.001. (**H**) Representative images of apoptotic TUNEL$^+$ cells in WT KIM-1 mice treated with Baf. Scale bar: 100 μm. (**I**) Quantification of *KIM-1* mRNA expression in post–I/R injury KIM-1 and KIM-1$^{\Delta mucin}$ kidneys (n = 3). *P < 0.05; ***P < 0.001. (**J**) Quantification of luminal cellular debris in post–I/R injury WT KIM-1 and KIM-1$^{\Delta mucin}$ mice (n = 3). **P < 0.01. (**K**) Representative images of luminal debris (arrows) in KIM-1 and KIM-1$^{\Delta mucin}$ mice after I/R injury. Scale bar: 25 μm. Statistical comparisons were calculated by 2-tailed Student's t test for the left 2 bars in **B** and by ANOVA followed by Bonferroni's post-hoc analysis for all other panels. Δmucin, KIM-1$^{\Delta mucin}$; WT, WT KIM-1.

No significant difference was detected in cisplatin-mediated apoptosis (Figure 2H) or H_2O_2-mediated LDH release (Figure 2I) between WT- and KIM-1$^{\Delta mucin}$–isolated PTCs in primary culture. We also detected no difference in apoptosis between WT and KIM-1$^{\Delta mucin}$ primary PTCs exposed to TNF-α (40 ng/ml) for 24 hours (data not shown). These data provide further confirmation that the protection by WT KIM-1 observed in vivo was not due to differences in epithelial cell susceptibility to cisplatin toxicity or susceptibility to TNF-α, one of the factors implicated in post-ischemic epithelial cell injury.

Differential susceptibility to ischemia between WT and KIM-1$^{\Delta mucin}$ mice is intrinsic to the kidney. Since KIM-1 has been reported to be expressed at low levels on T and B lymphocytes (18, 19), we next determined the relative importance of tubular cells versus BM-derived KIM-1 in the pathogenesis of kidney I/R injury by generating chimeric mice. Two approaches were used. BM chimeric mice were produced by transplanting WT KIM-1 BM cells into irradiated KIM-1$^{\Delta mucin}$ recipients (KIM-1$^{\Delta mucin}$ BM^{WT}) or KIM-1$^{\Delta mucin}$ BM cells into WT mice (KIM-1^{WT} BM$^{KIM\text{-}1\Delta mucin}$). Two additional groups of mice were produced with WT KIM-1 present on all cells (KIM-1^{WT} BM^{WT}) or with KIM-1$^{\Delta mucin}$ on all cells (KIM-1$^{\Delta mucin}$ BM$^{KIM\text{-}1\Delta mucin}$). Eight weeks after BM transplantation, the chimeric mice were subjected to I/R injury.

As shown in Figure 3, A and B, KIM-1$^{\Delta mucin}$ mouse kidneys showed more severe kidney injury, as measured by changes in serum creatinine (SCr) levels and histology, independent of whether their BM was reconstituted with WT or KIM-1$^{\Delta mucin}$ BM cells. KIM-1$^{\Delta mucin}$ recipient mice reconstituted with KIM-1$^{\Delta mucin}$ BM cells had slightly, but not significantly, increased SCr levels and tubulointerstitial damage compared with KIM-1$^{\Delta mucin}$ mice with WT BM cells. These data indicate a predominant role of intrinsic KIM-1 in protection against I/R injury.

In another set of experiments, RAG1-KO mice (*Rag1*$^{-/-}$) were crossed with *KIM-1*$^{\Delta mucin}$ mice. The *Rag1*$^{-/-}$ *KIM-1*$^{\Delta mucin}$ mice and *Rag1*$^{-/-}$ *KIM-1*^{WT} mice were used as recipients of spleen-derived B (B220$^+$) and T cell (CD3$^+$) transfusions from WT and KIM-1$^{\Delta mucin}$ mouse donors. Lymphocytes from KIM-1 or KIM-1$^{\Delta mucin}$ mice were incorporated into the spleen and found in the blood of *Rag1*$^{-/-}$ *KIM-1*$^{\Delta mucin}$ mice (Figure 3C). Lymphocyte reconstitution was found to be similar among all groups (data not shown). Three days after transfer, the chimeric mice were subjected to I/R injury. KIM-1$^{\Delta mucin}$ lymphocytes did not recapitulate the KIM-1$^{\Delta mucin}$ kidney's enhanced susceptibility to I/R injury, and lymphocytes from WT mice had little effect on reducing susceptibility to I/R injury in KIM-1$^{\Delta mucin}$ mice (Figure 3, D and E).

Consistent with the absence of a significant effect of KIM-1$^{\Delta mucin}$ BM-derived cells, it has been reported that there were very few differences found in the activity of T lymphocytes between WT and KIM-1$^{\Delta mucin}$ mice of the same age used in this study (17). There was slightly increased IFN-γ production after activation with either plate-bound anti-CD3/CD28 or CD11c$^+$ DCs in the presence of soluble anti-CD3 (ref. 17 and data not shown).

Increased innate immune inflammatory response in KIM-1$^{\Delta mucin}$ I/R-injured kidneys. Since phagocytic clearance of apoptotic cells by professional phagocytes has been shown to be important in modulating the immune response (20–22), we evaluated whether the increased tubulointerstitial damage, with reduced KIM-1–mediated phagocytosis seen in KIM-1$^{\Delta mucin}$ mice, was associated with quantitatively increased renal inflammation after I/R injury. Anti-Ly6G, anti-F4/80, and anti-CD3 Ab immunostaining was used to detect the influx of granulocytes, macrophages, and T lymphocytes, respectively, in the injured kidneys. We used cell counting rather than assessment of immune cells in the total kidney mass by methods such as flow cytometry because of the well-known differences in intrarenal localization of I/R injury–induced inflammatory cell infiltration. Immune inflammatory cells are primarily in the outer medulla, which comprises only a fraction of the total kidney mass. As shown in Figure 4A, kidneys from WT mice showed an abrupt increase in granulocyte infiltration, peaking on day 1 after I/R injury, followed by a later macrophage influx that was clearly detectable by day 3 after the insult. The KIM-1$^{\Delta mucin}$ I/R-injured kidneys, however, showed significantly greater amounts of tissue granulocytes and macrophages at both 1 and 3 days after injury (Figure 4A) and at 2 days after cisplatin injury (Figure 4B). In addition, more tubulitis was apparent in the I/R-exposed KIM-1$^{\Delta mucin}$ mice, with granulocytes and vesicle-rich macrophages infiltrating into the tubular wall as well as into the tubular basement membrane (Figure 4, C and D). Many breaks were apparent in the basement membrane in the KIM-1$^{\Delta mucin}$ I/R-injured kidneys, with macrophages present in intraluminal casts (Figure 4D, right panel arrows). The amount of T lymphocyte influx started to increase on day 3 after I/R injury and on day 2 after cisplatin injection, with no significant differences seen between the KIM-1$^{\Delta mucin}$ and WT kidneys (Figure 4, A and B). Flow cytometric analysis, using established methods with whole-kidney digestion (9, 23, 24), confirmed that KIM-1$^{\Delta mucin}$ mice tend to have more CD45$^+$ immune cell infiltration when normalized per gram of tissue. The relative proportion of different subsets of infiltrating cells — GR1$^+$, F4/80$^+$, CD3$^+$, B220$^+$, CD11c$^+$, and NK1.1$^+$ — was similar between WT and KIM-1$^{\Delta mucin}$ kidneys, indicating a general increase in immune infiltrates (Supplemental

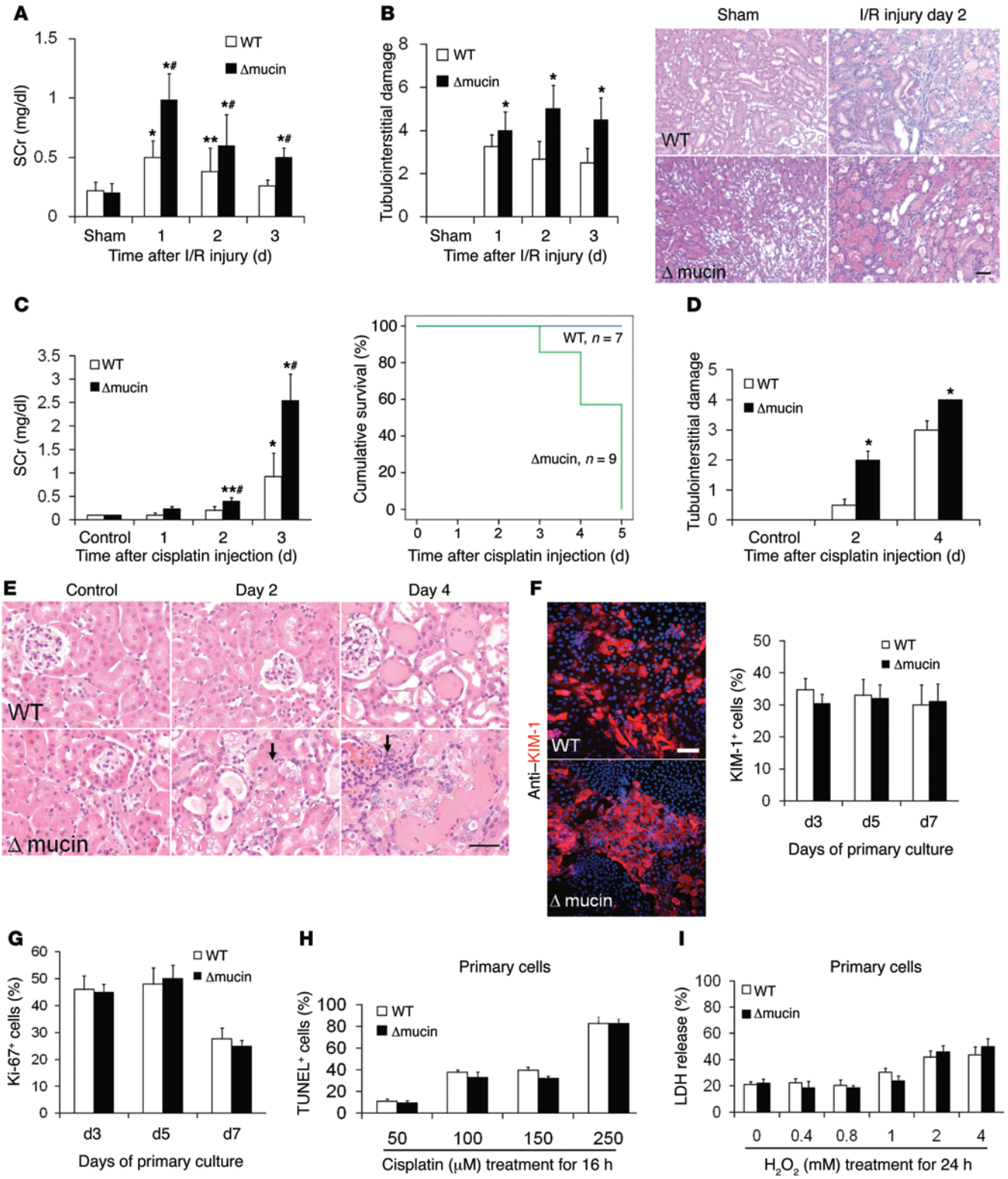

Figure 2. The KIM-1$^{\Delta mucin}$ mouse kidney is more susceptible to acute injury. (**A**) Changes in SCr over time after I/R injury in WT KIM-1 and KIM-1$^{\Delta mucin}$ mice (n = 12/time point/group). *P < 0.001 and **P < 0.05 vs. sham; #P < 0.05 vs. KIM-1 WT. (**B**) Quantification of tubulointerstitial damage (n = 3/time point/group) and H&E-stained histological images of I/R kidneys. *P < 0.05. (**C**) Changes in SCr (n = 6/group) and mortality over time after cisplatin injection into KIM-1 and KIM-1$^{\Delta mucin}$ mice. *P < 0.001 and **P < 0.05 vs. control; #P < 0.05 vs. KIM-1 WT. (**D** and **E**) Cisplatin-induced acute toxic kidney injury. Quantification of tubulointerstitial damage is shown in **D** and H&E-stained histological images in **E** (n = 3/group). *P < 0.05. (**F**) KIM-1 immunostaining using Abs targeting the extracellular domain of KIM-1 and percentage of KIM-1$^+$ cells in primary PTCs from KIM-1 and KIM-1$^{\Delta mucin}$ mice. Scale bar: 50 μm. (**G**) Percentage of Ki67$^+$ primary PTCs from KIM-1 and KIM-1$^{\Delta mucin}$ mice over time in primary culture. (**H**) TUNEL in situ hybridization of PTCs after a 16-hour incubation with various doses of cisplatin. (**I**) LDH released from PTCs after exposure to H_2O_2 at various doses (n = 3). Statistical comparisons were calculated by ANOVA followed by Bonferroni's post-hoc analysis. (**F**–**I**) No statistical differences between WT KIM-1 and KIM-1$^{\Delta mucin}$ groups.

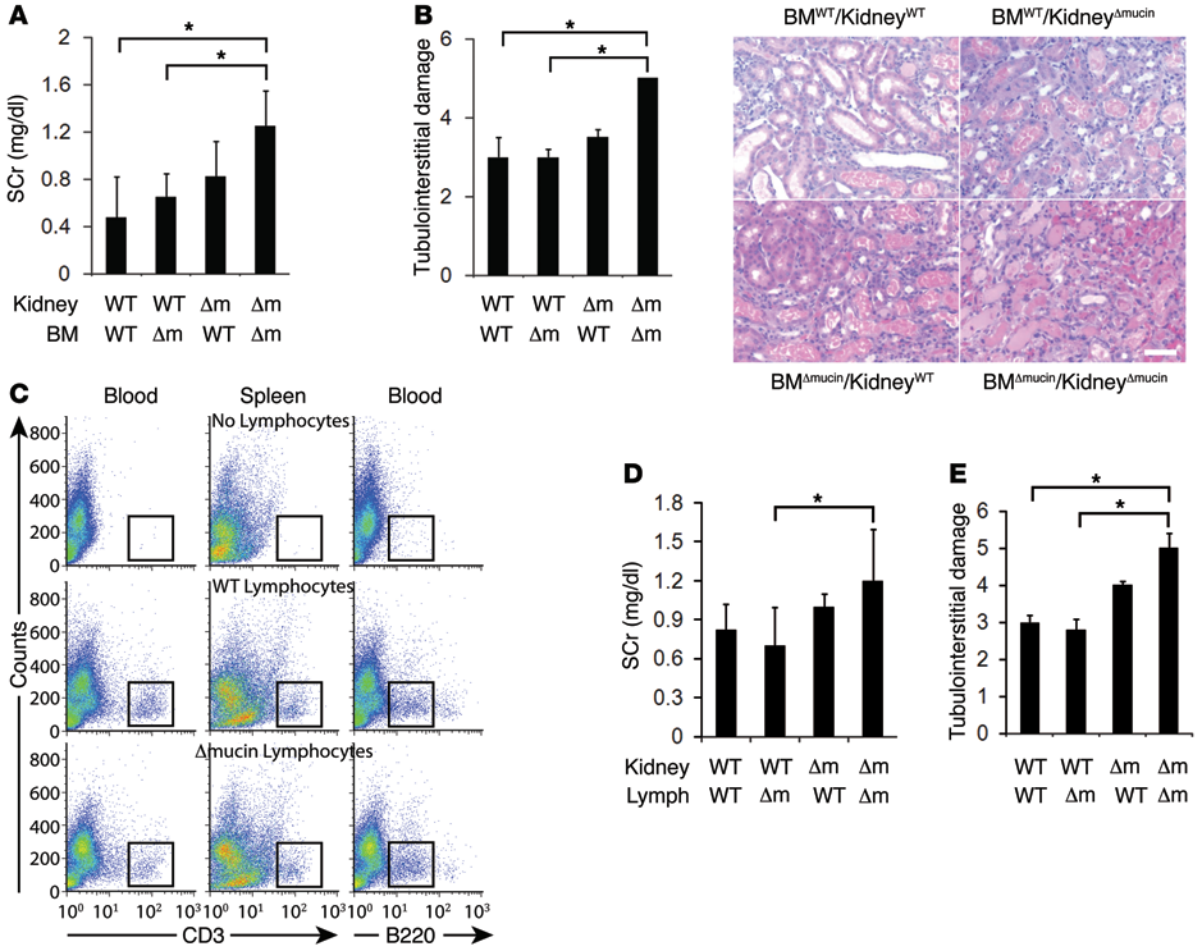

Figure 3. Kidney parenchymal cell KIM-1$^{\Delta mucin}$ expression predisposes to more severe I/R kidney injury. (**A**) SCr levels and (**B**) H&E-stained histological images and quantification of tubulointerstitial damage 1 day after I/R in different BM-transplanted chimeric mice groups (n = 6 animals/group). *P < 0.05. Scale bar: 50 μm. (**C**) Flow cytometric assay showing the presence of T and B lymphocytes in blood and spleens from *Rag1*$^{-/-}$ *KIM-1*$^{\Delta mucin}$ mice transfused with lymphocytes from WT KIM-1 or KIM-1$^{\Delta mucin}$ mice (plots are representative of 3 mice). (**D**) SCr levels and (**E**) quantification of tubulointerstitial damage 1 day after I/R in different lymphocyte-transfused *Rag1*$^{-/-}$ chimeric mouse groups (n = 5 animals/group). *P < 0.05. Statistical comparisons were calculated by ANOVA followed by Bonferroni's post-hoc analysis. Δm, KIM-1$^{\Delta mucin}$; WT, WT KIM-1.

Figure 1; supplemental material available online with this article; doi:10.1172/JCI75417DS1).

Consistent with the increased amount of granulocyte and macrophage infiltration, the mRNA levels of whole-kidney proinflammatory cytokine and chemokine genes encoding the proteins IL-1β, IL-6, TNF-α, and MCP1 (*Il1b*, *Il6*, *Tnfa*, and *Ccl2*) were significantly higher in KIM-1$^{\Delta mucin}$ I/R-injured and cisplatin-injured kidneys than in WT kidneys (Figure 5, A and B). MCP1 protein levels were elevated in KIM-1$^{\Delta mucin}$ post-ischemic kidneys compared with levels in WT kidneys (data not shown).

TLRs are well known to play critical roles in triggering and amplifying the innate immune response. As shown in Figure 5C, in WT I/R kidneys, there was upregulation of whole-kidney levels of mRNA encoding TLR2 and TLR4 on day 3 after injury, while KIM-1$^{\Delta mucin}$ kidneys showed significantly higher levels of mRNA encoding TLR2 and TLR4 at 1 and 3 days after I/R injury when compared with mRNA levels in WT kidneys. In the cisplatin toxic model, KIM-1$^{\Delta mucin}$ kidneys also showed much greater increases in *Tlr4* gene expression than were seen in kidneys of WT mice (Figure 5C). Immunostaining localized the expression of TLR4 mainly to the tubular epithelial cells (Figure 5D). TLR2 upregulation was localized mainly in the interstitial compartment as assessed by immunostaining for TLR2 (data not shown). We observed no obvious increases in mRNA levels of the 4 other *Tlr* genes (1, 3, 7, 9) after I/R injury in either WT or KIM-1$^{\Delta mucin}$ animals (data not shown). CSF-1 is a major cytokine involved in the recruitment, expansion, and differentiation of macrophages (25). It has recently has been shown that tubular CSF-1 is involved in the expansion of macrophages in AKI (26). CSF-1 was found to be upregulated at the mRNA level in KIM-1$^{\Delta mucin}$ kidneys compared with levels in WT kidneys (Figure 5E). These data strongly suggest that the innate immune response was greater in KIM-1$^{\Delta mucin}$ mice than in WT mice after I/R or acute cisplatin toxic kidney injury.

Expression of WT KIM-1 in kidney epithelial cells in vitro is associated with a decreased inflammatory phenotype. Tubular epithelial cells secrete proinflammatory cytokines and chemokines after injury, triggering and exacerbating inflammation (15, 27, 28). It remains unclear whether this tubular inflammatory reaction can be self-controlled or modulated. In proximal tubules isolated from the post-ischemic kidney, higher *Tlr4* gene expression was

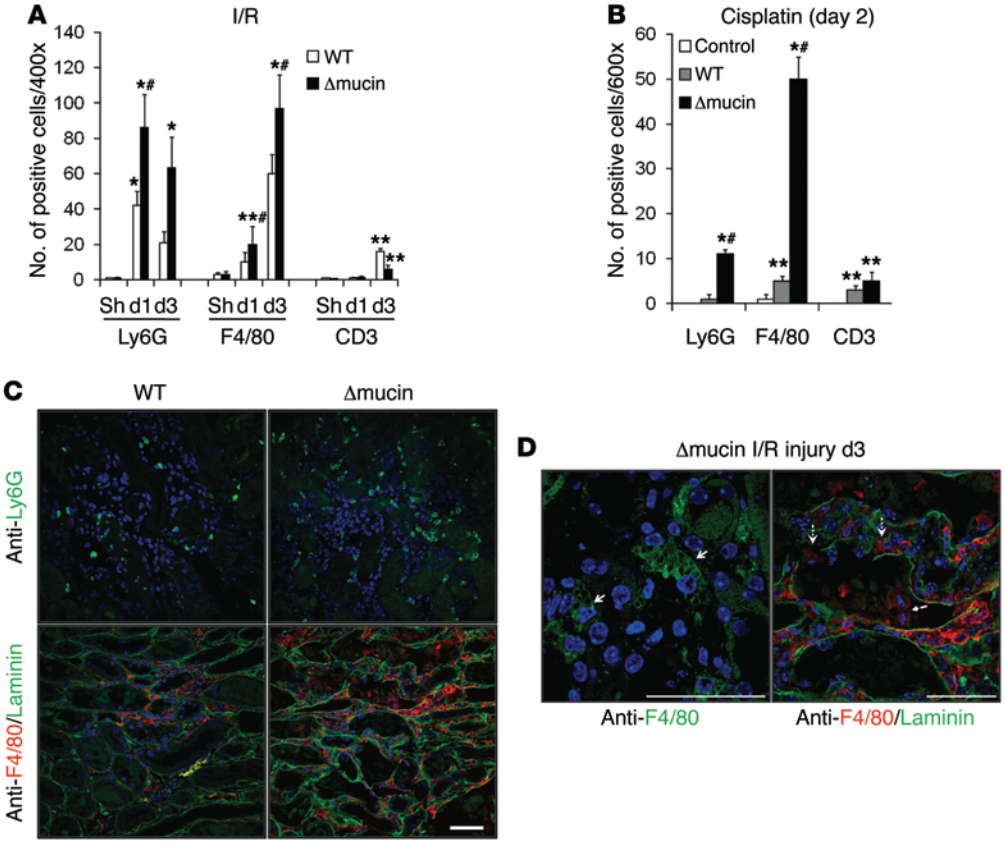

Figure 4. KIM-1$^{\Delta mucin}$ I/R-injured kidneys have more innate immune inflammatory infiltrates. Number of infiltrated granulocytes, macrophages, and T lymphocytes in I/R-injured kidneys on days 1 and 3 (**A**) and cisplatin-injured kidneys on day 2 (**B**) by immunostaining with anti-Ly6G, F4/80, and CD3 Abs (n = 3 mice/time point/group). $^{*}P < 0.001$ and $^{**}P < 0.05$ vs. sham; $^{\#}P < 0.01$ vs. WT. (**C**) Anti-Ly6G immunostaining and coimmunostaining for F4/80 (red) and laminin (green) in I/R-injured kidneys from KIM-1 WT and KIM-1$^{\Delta mucin}$ mice. (**D**) Coimmunostaining for F4/80 (red) and laminin (green) in KIM-1$^{\Delta mucin}$ I/R kidneys showed tubulitis with vesicle-rich macrophages infiltrating into the tubular wall (arrows in left panel) and broken tubular basement membrane with macrophages present in the casts (arrows in right panel). Images in **C** and **D** are representative of 3 animals per condition. Scale bars: 50 μm. Statistical comparisons were calculated by ANOVA followed by Bonferroni's post-hoc analysis. Sh, sham.

detected in the KIM-1$^{\Delta mucin}$ tubules compared with that in WT tubules (Figure 6A). Primary cultured PTCs expressing KIM-1$^{\Delta mucin}$ had higher levels of mRNA encoding TLR4 and MYD88 than did WT PTCs (Figure 6B). Tubular cells expressing WT KIM-1 showed much less TLR4 immunostaining and reduced secretion of the proinflammatory cytokines IL-6 and RANTES in response to LPS or LPS and IFN-γ (Figure 6, C and D). When LLC-PK1 cells were transfected with WT *KIM-1*, prefeeding with apoptotic cells reduced the LPS-induced increase in *Tlr4* mRNA levels when compared with the empty vector–transfected cells or KIM-1$^{\Delta mucin}$–expressing cells (Figure 6E).

Monocytes and macrophages are important effectors of the innate immune response after I/R injury in the kidney. We tested the effects of epithelial functional KIM-1 expression and phagocytosis on the activation of primary cultured BMMs by incubating BMMs with conditioned media from cells expressing WT or mutant KIM-1. After treatment with apoptotic bodies (APO) alone, TNF-α, TNF-α and APO, LPS, or LPS and APO, the supernatant from LLC-PK1 cells caused BMM activation as measured by proinflammatory cytokine production (Figure 7A shows TNF-α secretion as an example). Conditioned media from WT KIM-1–expressing LLC-PK1 cells, pre-fed with apoptotic cells alone or subsequently co-treated with TNF-α or LPS, significantly decreased BMM proliferation and production of TNF-α by BMMs (Figure 7, B and C) compared with control cells not expressing KIM-1 or cells expressing KIM-1$^{\Delta mucin}$. In dose titration experiments, using lentivirus expressing WT KIM-1, the greater the WT KIM-1 expression in LLC-PK1 cells, the more powerful the effect of the infected LLC-PK1 cell–conditioned media on decreasing TNF-α production in BMMs (Figure 7C). Thus, the expression of WT KIM-1 in PTCs potentiates a decreased proinflammatory phenotype, which is abrogated by loss of the phagocytic function of KIM-1 (KIM-1$^{\Delta mucin}$).

KIM-1 expression decreases the inflammatory response in kidney epithelial cells through downregulation of the NF-κB pathway. To determine the molecular mechanism by which KIM-1 expression modulates inflammatory signaling, we conducted DNA microarray analysis of PC3 human prostate cancer cells transduced with empty vector or KIM-1 (Figure 8). The genes that were significantly upregulated or downregulated by KIM-1 expression are listed in Supplemental Tables 1 and 2 and graphically displayed as a heatmap in Supplemental Figure 2. To determine which pathways were most likely to be involved in KIM-1 antiinflammatory signaling, the gene profile was analyzed using Ingenuity Pathway Analysis (IPA) software (QIAGEN) to generate molecular networks based on the differentially expressed genes (Figure 8). On the basis of the IPA, the major transcription factor predicted to be involved in the KIM-1 network was NF-κB (Figure 8). In particular, regulation of NF-κB by the phosphoinositide 3-kinase (PI3K) pathway member p85 stood out, because KIM-1 is known to directly bind to and regulate p85, and p85 has been shown to mediate KIM-1 signaling (16). In addition, p85 can suppress NF-κB activity (29, 30). Downmodulation of NF-κB can explain the dramatic reduction in TLR4 activity and the decreased proinflammatory cytokine release we observed in KIM-1–expressing cells. To test whether KIM-1 suppressed NF-κB, we examined NF-κB activity in vivo. KIM-1$^{\Delta mucin}$ kidneys had higher phosphorylated NF-κB (p–NF-κB) expression levels following I/R injury compared with levels in WT kidneys (Figure 9A). Expres-

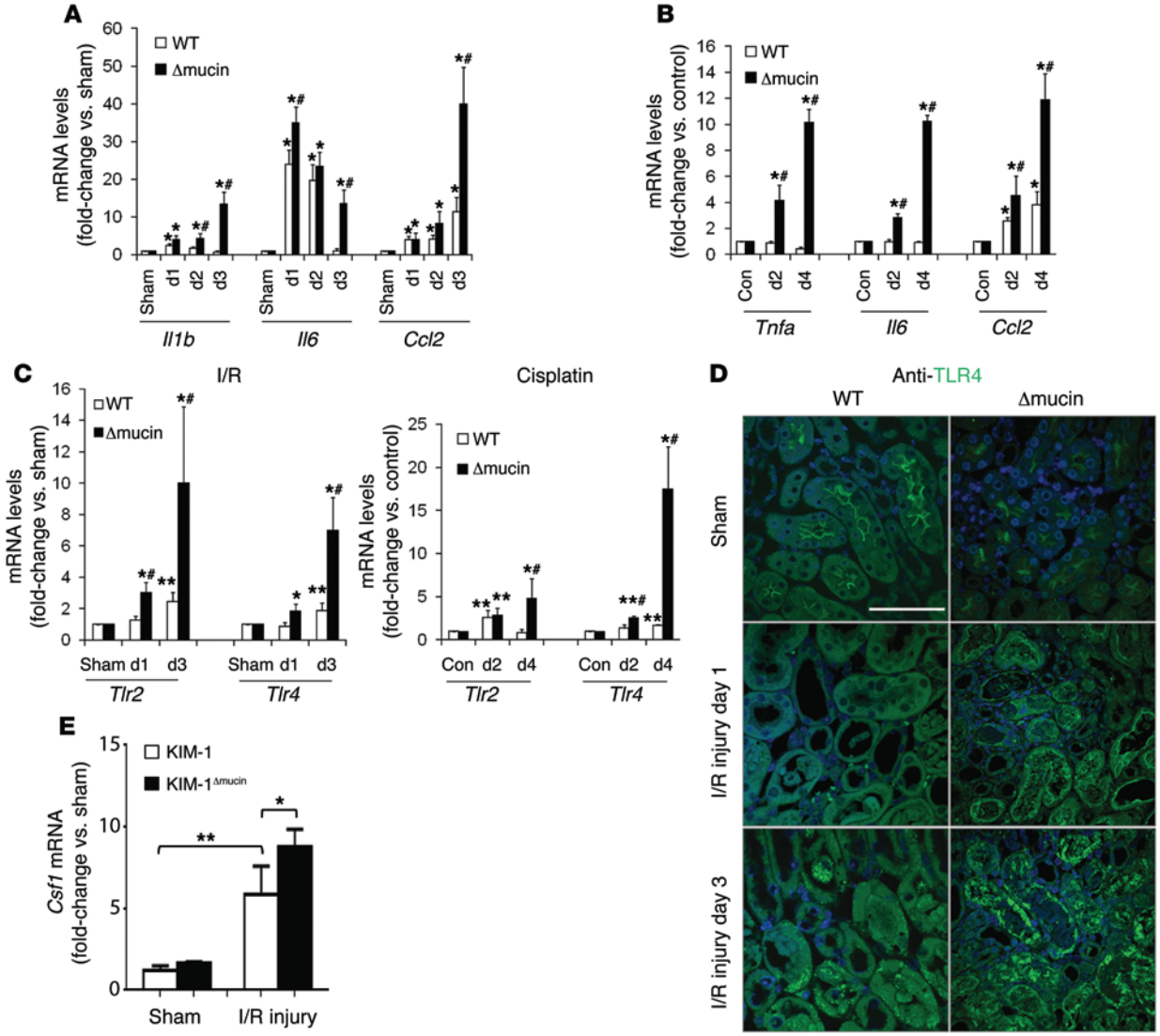

Figure 5. KIM-1$^{\Delta mucin}$ I/R-injured kidneys have greater inflammatory cytokine production. (**A**) *Il1b*, *Il6*, and *Ccl2* (IL-1β, IL-6, and MCP1) mRNA from whole I/R-injured kidneys, 1, 2, and 3 days after I/R and (**B**) *Tnfa*, *Il6*, and *Ccl2* (TNF-α, IL6, and MCP1) mRNA levels in cisplatin-injured kidneys in KIM-1 WT and KIM-1$^{\Delta mucin}$ mice (n = 3 mice/time point/group). *P < 0.05 vs. sham or control; #P < 0.05 vs. WT. (**C**) mRNA levels of *Tlr2* and *Tlr4* in I/R- and cisplatin-injured kidneys in KIM-1 WT and KIM-1$^{\Delta mucin}$ mice (n = 3 mice/time point/group). *P < 0.01 and **P < 0.05 vs. sham; #P < 0.01 vs. WT. (**D**) Anti-TLR4 immunostaining of I/R-injured kidneys from KIM-1 WT and KIM-1$^{\Delta mucin}$ mice (images are representative of 3 independent experiments). Scale bar: 50 μm. (**E**) *Csf1* mRNA levels in I/R-injured or sham kidneys from KIM-1 WT and KIM-1$^{\Delta mucin}$ mice. *P < 0.05; **P < 0.01 (n = 3). Statistical comparisons among groups were calculated by ANOVA followed by Bonferroni's post-hoc analysis. Con, vehicle control.

sion of KIM-1 reduced p–NF-κB in primary PTCs treated with INF-γ. The addition of apoptotic cells reduced LPS- or TNF-α–induced p–NF-κB levels in WT PTCs to a greater extent than in KIM-1$^{\Delta mucin}$–expressing cells (Figure 9B). To confirm the reduction in NF-κB signaling, we measured NF-κB activity using a luciferase reporter driven by an NF-κB–responsive element. Expression of WT KIM-1 in LLC-PK1 cells significantly reduced TNF-α–induced NF-κB activity when compared with induction in cells expressing KIM-1$^{\Delta mucin}$ (Figure 9C). NF-κB activity was further reduced with the addition of apoptotic cells (Figure 9C). These data indicate that WT KIM-1, but not KIM-1$^{\Delta mucin}$, downmodulates NF-κB, which was further reduced by phagocytosis of apoptotic cells.

In T cells, KIM-1 has been shown to interact with p85 and activate PI3K signaling in a phosphotyrosine-dependent manner (16). To determine the mechanism by which KIM-1 downmodulates NF-κB, we examined phosphorylation levels of WT KIM-1 and KIM-1$^{\Delta mucin}$. Lysates from HEK-293 cells expressing WT KIM-1 or KIM-1$^{\Delta mucin}$ were immunoprecipitated with anti-phosphotyrosine Ab, and the resulting precipitate was probed by immunoblotting for the presence of WT KIM-1 or KIM-1$^{\Delta mucin}$ (Figure 9D). WT KIM-1 showed prominent basal phosphorylation, which was not further enhanced by phagocytosing apoptotic cells. KIM-1$^{\Delta mucin}$ showed significantly less tyrosine phosphorylation in both basal and apoptotic cell–treated conditions compared with that detected in WT KIM-1 (Figure 9D). Next, we examined the interaction between p85 and WT KIM-1 or KIM-1$^{\Delta mucin}$. Cells were transfected with FLAG-tagged WT or *KIM-1$^{\Delta mucin}$*. Lysates were then immunoprecipitated with anti-FLAG Ab. The resulting precipitate was then probed for p85

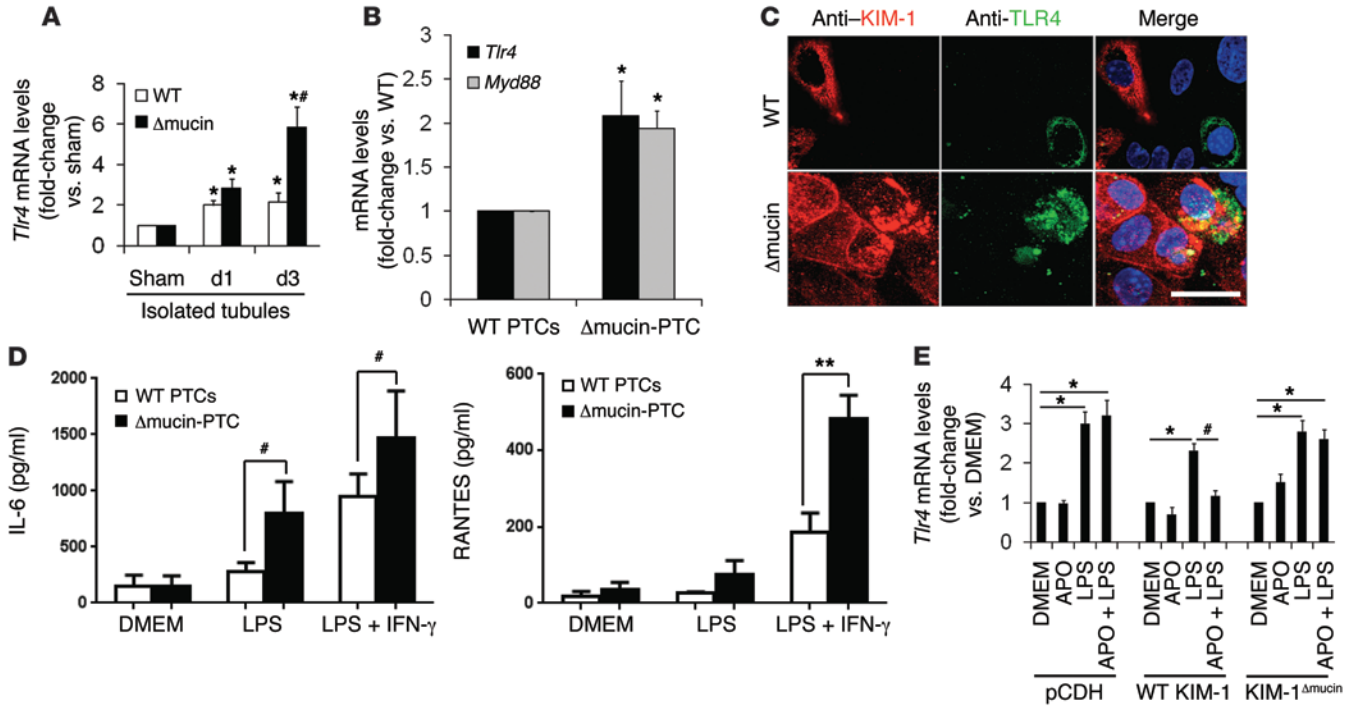

Figure 6. Expression of functional KIM-1 downmodulates inflammatory cytokine production by kidney epithelial cells. (**A**) *Tlr4* mRNA levels in tubules isolated from KIM-1 (WT) and KIM-1$^{\Delta mucin}$ I/R-injured kidneys 1 and 3 days after injury (n = 3 mice/time point/group). *P < 0.05 vs. sham; #P < 0.05 vs. WT. (**B**) *Tlr4* and *Myd88* mRNA levels in primary cultured tubular cells isolated from KIM-1 and KIM-1$^{\Delta mucin}$ kidneys. *P < 0.01. (**C**) Coimmunostaining for KIM-1 (red) and TLR4 (green) in primary cultured tubular cells isolated from KIM-1 or KIM-1$^{\Delta mucin}$ mouse kidneys after exposure to LPS. WT KIM-1–expressing cells did not show obvious TLR4 expression, whereas KIM-1$^{\Delta mucin}$–expressing cells showed increased intracellular TLR4 expression (images are representative of 3 independent experiments). Scale bar: 20 μm. (**D**) Secretion of IL-6 and RANTES by primary cultured tubular cells isolated from KIM-1 WT and KIM-1$^{\Delta mucin}$ kidneys. **P < 0.001; #P < 0.05 (n = 3). (**E**) *Tlr4* mRNA levels in LLC-PK1 cells transfected with pCDH empty vector, WT KIM-1, or KIM-1$^{\Delta mucin}$ (n = 5). With LPS treatment, the pCDH cells had increased *Tlr4* gene production, which did not change with apoptotic cell (APO) pre-feeding. Pre-feeding apoptotic cells to LLC-PK1 cells expressing WT KIM-1, but not KIM-1$^{\Delta mucin}$, markedly decreased *Tlr4* mRNA levels. *P < 0.01 and #P < 0.05. Statistical comparisons among groups were calculated by ANOVA followed by Bonferroni's post-hoc analysis.

by immunoblotting. WT KIM-1 was found to have a greater interaction with p85 when compared with KIM-1$^{\Delta mucin}$ (Figure 9E). To determine whether p85 was associated with KIM-1 phagocytosis, WT KIM-1–expressing LLC-PK1 cells were stained for KIM-1 and p85 (Figure 9F). We found that p85 localized to KIM-1^{+} phagosomes (Figure 9F, middle panels), but not in pCDH- or KIM-1$^{\Delta mucin}$–expressing cells (Figure 9F, left and right panels). To confirm that p85 colocalized with KIM-1 phagosomes, cells were imaged in a z series to make a 3D-reconstructed image. As shown in Figure 9G, a single z plane revealed colocalization of KIM-1 and p85, surrounding phagocytosed apoptotic cells. We used 3D reconstruction to examine a single apoptotic cell in the process of being phagocytosed and observed that p85 localized to the basal region of the KIM-1^{+} phagocytic cup (Figure 9H, right and lower panels). To determine whether KIM-1 downmodulation of NF-κB was p85 dependent, we examined the effect of KIM-1 overexpression in the presence of the PI3K inhibitors wortmannin and LY294002. WT KIM-1 PTCs had reduced basal p–NF-κB compared with that detected in KIM-1$^{\Delta mucin}$ cells treated with vehicle. Treatment with either wortmannin or LY294002 increased p–NF-κB in WT PTCs to levels similar to those in KIM-1$^{\Delta mucin}$ cells (Figure 9I). Taken together, these data suggest that KIM-1 expression downregulates inflammatory signaling through interaction with and activation of p85 and subsequent downmodulation of NF-κB activity (Figure 10).

Discussion

In the present study, we found that proximal tubular phagocytosis plays a major role in downregulation of the innate immune response to kidney injury. KIM-1 is the most upregulated protein in the proximal tubules after AKI (31) and is a phosphatidylserine receptor that mediates phagocytosis of apoptotic cells and oxidized lipids by renal PTCs (14). Our evidence indicates that surviving PTCs expressing KIM-1 will phagocytose luminal cellular debris, which consists of apoptotic and necrotic cells that are released into the lumen or that are as yet unreleased from the basement membrane. KIM-1–mediated clearance of apoptotic cells helped clear luminal obstruction and reduced the need for professional phagocytes, macrophages, and DCs to infiltrate the tubule lumen to clear the debris. Elimination of the mucin domain of KIM-1 in mice greatly reduced the phagocytic function of the protein. Baf blocked lysosomal clearance of phagocytosed apoptotic cells. Under these conditions, the number of TUNEL^{+} cells in WT KIM-1 kidneys after injury increased by approximately 10-fold, compared with only an approximate 2-fold increase of these cells in KIM-1$^{\Delta mucin}$ mice. Mice with this mutation had an increased susceptibility to ischemic injury and toxic exposure to cisplatin. The phagocytic clearance of apoptotic cells by intact KIM-1 triggered the interaction between KIM-1 and p85 and subsequently downregulated NF-κB activity, resulting

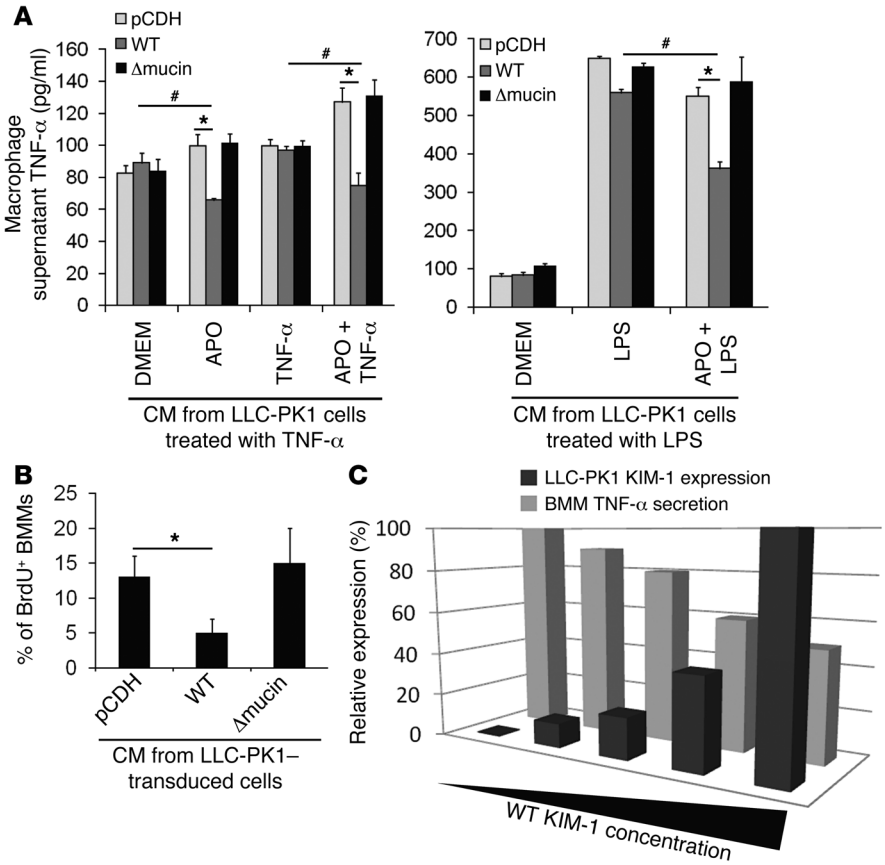

Figure 7. Expression of WT KIM-1, but not KIM-1$^{\Delta mucin}$, in kidney epithelial cells downregulates the activation of macrophages. (**A**) TNF-α secretion by BMMs exposed to conditioned media (CM) collected from LLC-PK1 cells expressing pCDH, WT KIM-1, or KIM-1$^{\Delta mucin}$ incubated with apoptotic cells or not and then treated with TNF-α or LPS without apoptotic cells before incubation (n = 5). $^{*}P < 0.01$; $^{\#}P < 0.05$. (**B**) Percentage of BrdU^{+} BMMs after a 24-hour treatment with conditioned media from LLC-PK1 cells expressing pCDH vector, WT KIM-1, or KIM-1$^{\Delta mucin}$ (n = 3). $^{*}P < 0.05$. (**C**) Relationship between WT KIM-1 expression in LLC-PK1 cells and TNF-α secretion by BMMs treated with conditioned media from these cells. The control was set as the LLC-PK1 group that had the highest level of KIM-1 expression or the BMM group that had the highest TNF-α secretion levels. The conditioned media from LLC-PK1 cells expressing KIM-1 had a dose-dependent effect on the decrease in TNF-α secretion by BMMs (n = 3). r = 0.916; P = 0.04. Groups were compared by ANOVA followed by Bonferroni's post-hoc analysis (**A** and **B**) and Spearman's rank correlation test (**C**). CM, conditioned media.

in an antiinflammatory phenotype in PTCs, including reduced TLR4 expression, proinflammatory cytokine production, and a decreased ability to activate macrophages. These effects that led to downregulation of the inflammatory response were prevented by the KIM-1$^{\Delta mucin}$ mutation (Figure 10).

The tubular epithelium is not merely a passive victim of injury, but also an active participant in the inflammatory response in AKI (27). In murine models of ischemic and toxic AKI, the early innate immune responses exacerbate inflammatory injury to the tissue (32). Downregulation of the innate immune response would serve as an important response of the tubule to alleviate inflammation and subsequent tubular damage. In addition to the generation of proinflammatory and chemotactic cytokines such as TNF-α, MCP-1, IL-6, IL-1β, and CSF-1, which activate macrophages, tubular cells also express TLR4 (33–36), which is one of the key mediators of the innate immune response after tissue injury or infection (37). *Tlr4*$^{-/-}$ mice are protected against ischemic injury (35, 36), and this protection was shown to be principally due to elimination of TLR4 in tubular cells (35). Our data indicate that this tubular proinflammatory reaction with increased TLR4 expression after acute injury can be modulated by KIM-1.

With the dramatic expression of KIM-1 and its potent ability to mediate phagocytosis, the renal proximal tubules act as native scavengers for clearing dead cells after acute tissue injury. KIM-1–expressing proximal tubules present a decreased proinflammatory phenotype after phagocytosis of apoptotic cells and consequently limit the acute inflammation. This reveals a natural defense system against acute tubular injury.

Recently, we have shown that conditional chronic expression of KIM-1 in renal epithelial cells resulted in spontaneous and progressive interstitial kidney inflammation with fibrosis, leading to chronic renal failure (15). In the unilateral ureteral obstruction (UUO) model, KIM-1$^{\Delta mucin}$ was protective against fibrosis (15). These results, together with the findings of the current study, raise an important question: What exactly is the role of KIM-1 in kidney injury? A primary function of KIM-1 is that of a scavenger receptor that facilitates uptake of apoptotic cells, oxidized lipids, necrotic debris (ref. 14 and data not shown), and possibly other components of the tubular lumen. KIM-1–mediated phagocytosis of apoptotic/necrotic debris, however, also induces downstream signaling in PTCs. Professional phagocytes such as macrophages and DCs are known to have differential reactions to various ligands. Uptake of apoptotic cells has been shown to produce an antiinflammatory response (20, 38), while phagocytosis of necrotic cells leads to proinflammatory signaling (39, 40), and uptake of oxidized lipids leads to cell stress and death (41). In this regard, the downstream effect of KIM-1–mediated phagocytosis will be dependent on the phagocytic ligand, which varies with injury: acute injury to the kidney is associated with the presence of many apoptotic cells, while chronic injury is associated with glomerular leakage and prolonged exposure to oxidized lipids and various protein products of cell debris (9, 27, 28). In the current study, phagocytosis of apoptotic cells was found to downregulate the proinflammatory response in KIM-1–expressing cells. Mechanistically, KIM-1 WT, but not KIM-1$^{\Delta mucin}$, interacted with p85, a known regulator of NF-κB (29, 30). KIM-1–mediated phagocytosis decreased NF-κB activity in

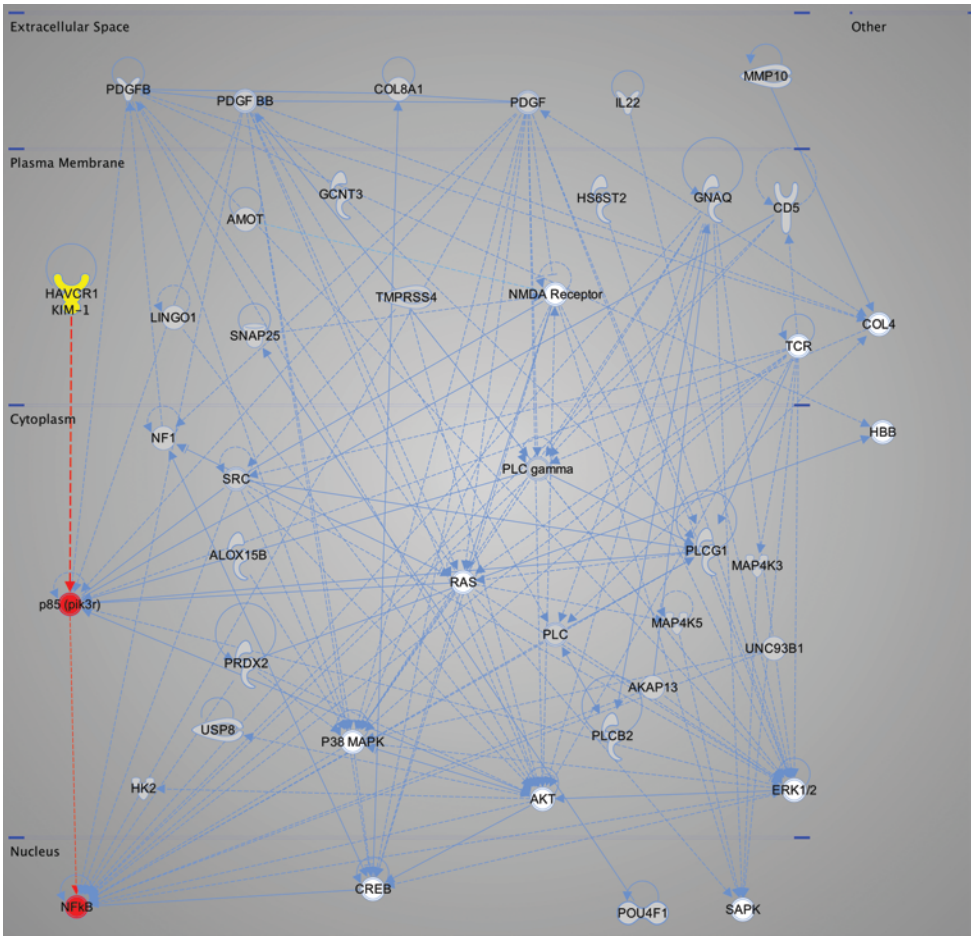

Figure 8. IPA interaction network generated from microarrays comparing expression patterns between PC3 cells expressing KIM-1 and cells expressing β-galactosidase. The network was generated from an analysis of the genes listed in Supplemental Tables 1 and 2. The genes labeled in gray and KIM-1 (HAVCR1) are from the microarray analysis. The genes labeled in white and red are predicted to be involved on the basis of IPA analysis.

a p85-dependent manner. Thus, in the context of AKI, with substantial apoptotic cell death (27, 28), tubular KIM-1 phagocytosis of apoptotic bodies resulted in a dominant antiinflammatory phenotype in the renal tubules. In contrast, chronic KIM-1 expression on both luminal and basolateral aspects of the cell due to loss of cell polarity resulted over time in enhanced tubular cell injury and triggered a more robust inflammatory response in KIM-1–expressing tubular cells (15). In various chronic kidney diseases, loss of the glomerular filtration barrier facilitates exposure of KIM-1$^+$ cells to oxidized lipids, various urinary proteins, and other ligands and triggers a proinflammatory phenotype. Thus, acute expression of tubular KIM-1 after AKI protects against inflammatory tissue injury, while chronic sustained KIM-1 expression, as seen in our *KIM-1*–transgenic animal model (15), results in chronic inflammation and fibrosis. This is supported by the fact that in the reversible moderate I/R injury mouse model, in which there is very little chronic fibrosis, KIM-1 expression is mainly enhanced after the acute injury, but then rapidly declines during the remodeling phase (12). By contrast, in chronic injury, absence of the mucin domain is protective, as reflected by the fact that KIM-1$^{\Delta mucin}$ mice are resistant to chronic injuries such as UUO (15).

KIM-1/TIM-1 has been implicated in the activation of Th2, Th1, and Th17 differentiation (18, 42), as well as in the activation of B cells, DCs, and NK T cells (18, 19, 43). T cells are known to contribute to inflammation in AKI (11), whereas B cells are reported to be involved in the repair process after kidney I/R injury (44). A recent study of KIM-1–deficient animals, however, failed to find any significant effect on T lymphocyte activation, proliferation, or cytokine production (42). In the present study, we evaluated whether the enhanced injury in KIM-1$^{\Delta mucin}$ mice could be mimicked by transplantation of KIM-1$^{\Delta mucin}$ BM into WT mice. In BM chimeric and splenic chimeric mice, lymphocytes from WT or KIM-1$^{\Delta mucin}$ mice did not significantly change the susceptibility of the WT or KIM-1$^{\Delta mucin}$ recipient animals to kidney I/R injury. Furthermore, our in vitro results confirmed that KIM-1$^{\Delta mucin}$ T lymphocytes did not have a distinct abnormality compared with WT lymphocytes (data not shown). Thus, functional KIM-1 expression in kidney parenchymal cells protects against inflammation and tissue damage during AKI. Two studies have demonstrated a partial protection of the kidneys by the low-avidity antagonist anti–TIM-1 Ab RMT1-10 in AKI induced by I/R or cisplatin and concluded that benefits of inhibiting TIM-1 derive from T cell effects (45, 46). Questions have been raised, however, concerning the specificity of the RMT1-10 Ab (47).

Our studies provide a rationale for the extremely robust character of upregulation of KIM-1 early after kidney injury in humans and in many other species of animals. The presence of a large amount of apoptotic cellular debris requires rapid clearance before it becomes proinflammatory. In addition to this clearance function, the process of KIM-1–mediated PTC uptake of the apoptotic debris itself serves an antiinflammatory function. By contrast, in chronic kidney disease, the endocytic function of KIM-1 becomes maladaptive.

In summary, we demonstrate that KIM-1–mediated phagocytosis, which is dependent on the presence of the mucin domain of the protein, enables the kidney proximal tubular epithelial cell to be a potent immunosuppressive downregulator of the innate immune response that is activated in AKI. Facilitation of the phagocytic process could represent a new therapeutic approach for AKI therapy in the future.

Methods

Animals

C57BL/6 and RAG1-KO (*Rag1*$^{-/-}$ on a C57BL/6 genetic background) mice were purchased from The Jackson Laboratory. *KIM-1*$^{\Delta mucin}$ mice on a C57BL/6 genetic background were generated by replacing exon 3 of the *KIM-1* gene with a *PGK* promoter–driven neomycin-resistance cassette, which resulted in KIM-1 proteins without the mucin domain (17). Mice homozygous for the *mKIM-1*$^{\Delta 130-189}$ gene were generated by interbreeding the heterozygotes. The littermates were used as WT controls. *Rag1*$^{-/-}$ mice were crossed with *KIM-1*$^{\Delta mucin}$ mice to generate *Rag1*$^{-/-}$ *KIM-1*$^{\Delta mucin}$ mice. Eight- to twelve-week-old male mice were used for the experiments.

Induction of AKI in mice

Ischemia for 25 minutes at 37°C was induced in both kidneys using the flank approach as previously reported (48). Warm saline (1 ml at 37°C) was injected i.p. after surgery for volume supplementation. Sham operations were performed with exposure of both kidneys, but without induction of ischemia. Cisplatin toxic AKI was induced by a 1-time 20 mg/kg i.p. injection of cisplatin (Sigma-Aldrich) in PBS. In some experiments, Baf was administered as a 1-time 1 mg/kg i.p. injection 1 hour before induction of ischemia. The control animals were administered the same amount of PBS.

Renal function and histology

Plasma creatinine was determined by the picric acid method (49). Kidney histology was examined in formalin-fixed, H&E-stained sections. The degree of tubulointerstitial damage was scored semiquantitatively on a 0 to 5+ scale, according to the percentage of the outer medulla area affected by tubular necrosis and/or apoptosis, loss of brush border, tubular atrophy, and tubular dilation (0 = no lesion, 1+ = <25%, 2+ = >25% to 50%, 3+ = >50% to 75%, 4+ = >75% to <100%, 5+ = 100%).

Generation of BM chimeric mice

BM cells were collected from WT and KIM-1$^{\Delta mucin}$ mice by flushing femurs and tibiae with RPMI 1640 containing 5% FCS. Recipient mice were lethally irradiated with a single dose of 9.5 Gy from a cesium source using a 137Cs irradiator (Gammacell 40 Exactor; Nordion). Six hours after irradiation, recipient irradiated mice were injected via the tail vein with 10×10^6 BM cells. Chimeras were generated by the following donor-recipient combinations: KIM-1$^{\Delta mucin}$ → WT (reconstitution of WT mice with BM from KIM-1$^{\Delta mucin}$ mice); KIM-1$^{\Delta mucin}$ → KIM-1$^{\Delta mucin}$; WT → KIM-1$^{\Delta mucin}$; and WT → WT (sham) (n = 6 animals/group). The animals were allowed to recover for 9 weeks to ensure stable engraftment. Twenty-five minutes of bilateral kidney ischemia and 24, 48, and 72 hours of reperfusion were performed on these chimeric mice.

Generation of splenic lymphocytes in chimeric mice

Splenic B and T cells isolated from WT or KIM-1$^{\Delta mucin}$ mice were transferred into *Rag1*$^{-/-}$ *KIM-1*$^{\Delta mucin}$ or *Rag1*$^{-/-}$ *KIM-1*^{WT} mice. Single-cell suspensions from spleens were prepared according to standard methods, and erythrocytes were lysed with ACK (ammonium-chloride-potassium) Lysing Buffer (BioWhittaker, Lonza Group). Lymphocytes (including both T and B lymphocytes) from donors were purified by magnetic bead positive separation (anti-CD3, clone 17A2 and anti-B220, clone RA3-6B2 Abs; Miltenyi Biotec). Recipient mice were injected via the tail vein with 20×10^6 splenic lymphocytes. Chimeric mice were produced (n = 5 animals/group) as follows: KIM-1^{WT} lymph^{WT}, KIM-1^{WT} lymph$^{KIM\text{-}1\Delta mucin}$, KIM-1$^{\Delta mucin}$ lymph^{WT}, and KIM-1$^{\Delta mucin}$ lymph$^{KIM\text{-}1\Delta mucin}$. Three days after lymphocyte infusion, the chimeric mice were subjected to I/R injury. Engraftment of the infused lymphocytes was verified by flow cytometric assay to detect the existence of CD3$^+$ and CD20$^+$ lymphocytes in peripheral blood and isolated splenic cells.

Isolation of tubules from kidney

The kidney cortex was dissected, diced, and digested in DMEM containing Liberase CI (40 μg/ml; Roche Diagnostics) using a gentleMACS Dissociator (Miltenyi Biotec). The enzyme reaction was terminated with cold horse serum, then the tubule suspension was passed sequentially through 40- and 70-μm cell meshes (Falcon; BD Diagnostics). Tubules were collected with cold PBS from the 70-μm mesh, and protein and RNA were extracted immediately.

FACS of kidney cells

The kidney cortex was dissected, diced, and digested in DMEM containing Liberase CI (40 μg/ml) using a gentleMACS Dissociator. The enzyme reaction was terminated with cold horse serum, then the tubule suspension was passed through 40-μm Falcon meshes. The single isolated kidney cells were stained with anti–KIM-1 and anti-TLR4 Abs and analyzed using the FACSCaliber Analyzer (BD Biosciences).

Flow cytometry

Mice were anesthetized, sacrificed, and perfused with ice-cold PBS via the left ventricle for 2 minutes. Kidneys were minced and incubated with collagenase type IA (10 μg/ml) (Sigma-Aldrich) in DMEM/F12 for 20 minutes at 37°C with constant shaking. Digestion was stopped by the addition of ice-cold FBS. The digested kidney tissue suspension was passed through a 100-μm cell strainer (Thermo Fisher) and centrifuged at 1,000 *g* for 5 minutes at 4°C. The pellet was then incubated with ACK Lysing Buffer (0.15 M NH_4Cl, 10 mM $KHCO_3$, and 0.1 mM Na_2 EDTA) for 5 minutes at room temperature, to remove rbc, and centrifuged at 1,000 *g* for 5 minutes at 4°C. The pellet was then washed with PBS containing 1% BSA and 0.1% sodium azide (Sigma-Aldrich) and passed through a 40-μm cell strainer. Cells were incubated with anti-mouse CD16/32 to block nonspecific Fc binding, then incubated with anti-mouse CD45 (FITC: 30-11F, BD Pharmingen; APC: 30-F11, BioLegend) plus fluorochrome-conjugated Abs against mouse GR1 (RB6-8C5; BD Pharmingen); F4/80 (BM8; BioLegend); CD3 (17A2; BD Pharmingen); B220 (RA3-6B2; eBioscience); CD11c (Biolegend, N418); and NK1.1 (PK 136; BD Pharmingen). Data were acquired using a BD FACSCanto and analyzed using FlowJo software.

Primary culture of PTCs

Primary cultures of kidney PTCs from both WT KIM-1 and KIM-1$^{\Delta mucin}$ mouse kidneys were generated using established methods (14). Briefly, the kidney cortex was dissected, diced, and then digested in a solution of collagenase (15 μg/ml) for 30 minutes at 37°C. The enzyme reaction was terminated with horse serum. Glomeruli and remaining tissue clumps were separated by decanting after 2 minutes of gravity sedimentation. After washing 2 times in PBS, tubules were resuspended in tubule medium (DMEM/F-12 with transferrin, insulin, selenium, hydrocortisone, and EGF) and aliquoted into collagen I–coated tissue culture–grade dishes con-

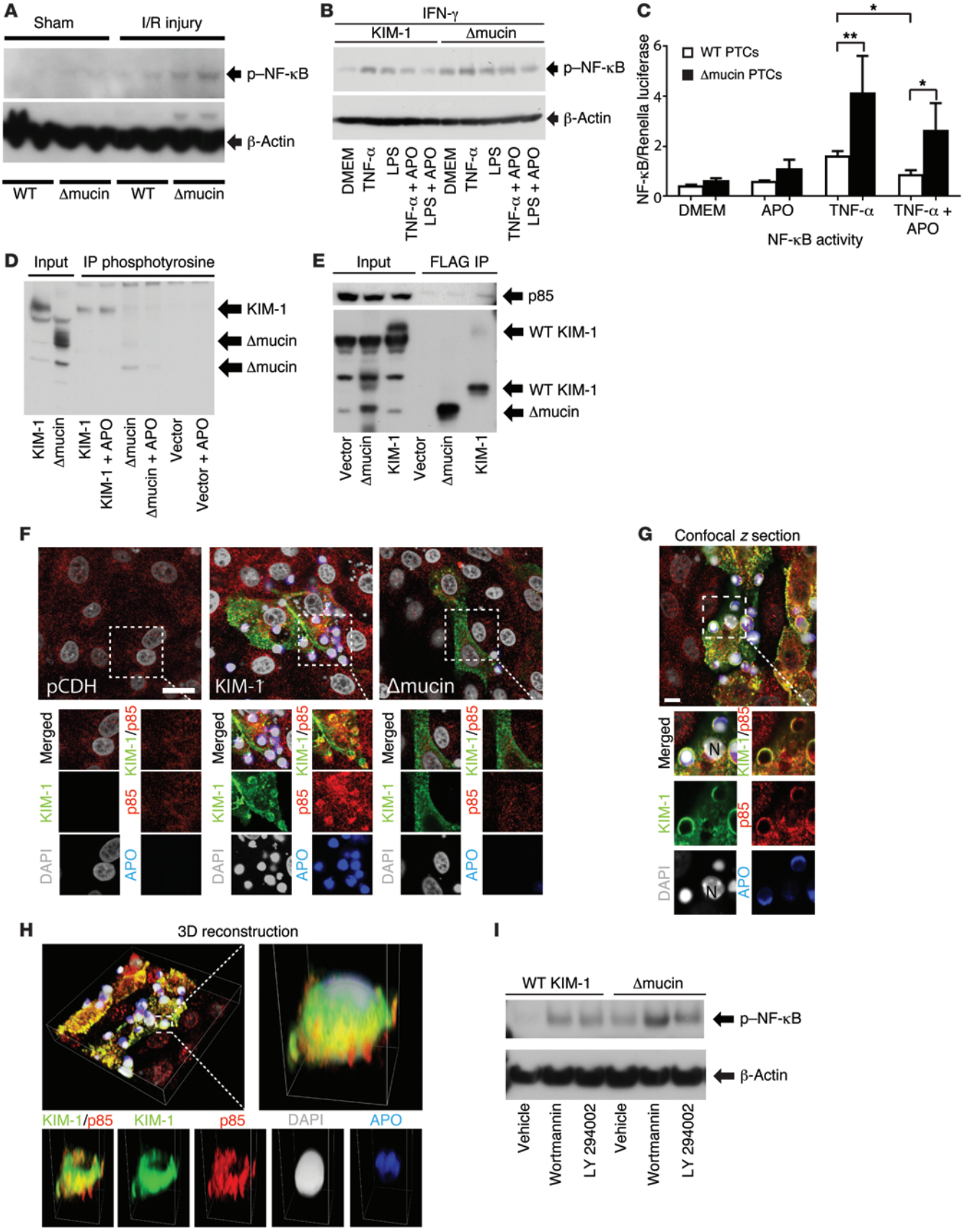
A
Sham
I/R injury
p–NF-κB
β-Actin
WT
Δmucin
WT
Δmucin
B
IFN-γ
KIM-1
Δmucin
p–NF-κB
β-Actin
DMEM
TNF-α
LPS
TNF-α + APO
LPS + APO
DMEM
TNF-α
LPS
TNF-α + APO
LPS + APO
C
WT PTCs
Δmucin PTCs
NF-κB/Renella luciferase
0
2
4
6
*
**
*
DMEM
APO
TNF-α
TNF-α + APO
NF-κB activity
D
Input
IP phosphotyrosine
KIM-1
Δmucin
Δmucin
KIM-1
Δmucin
KIM-1
KIM-1 + APO
Δmucin
Δmucin + APO
Vector
Vector + APO
E
Input
FLAG IP
p85
WT KIM-1
WT KIM-1
Δmucin
Vector
Δmucin
KIM-1
Vector
Δmucin
KIM-1
F
pCDH
KIM-1
Δmucin
Merged
KIM-1/p85
KIM-1
p85
DAPI
APO
G
Confocal z section
Merged
KIM-1/p85
KIM-1
p85
DAPI
APO
N
N
H
3D reconstruction
KIM-1/p85
KIM-1
p85
DAPI
APO
I
WT KIM-1
Δmucin
p–NF-κB
β-Actin
Vehicle
Wortmannin
LY 294002
Vehicle
Wortmannin
LY 294002

Figure 9. Expression of WT KIM-1, but not KIM-1$^{\Delta mucin}$, in PTCs downregulates NF-κB activity in a PI3K-dependent manner. (**A**) Immunoblot analysis of p–NF-κB in I/R kidneys from WT KIM-1 or KIM-1$^{\Delta mucin}$ mice (n = 4 animals). (**B**) p–NF-κB expression in WT KIM-1 or KIM-1$^{\Delta mucin}$ primary PTCs (representative of 4 experiments). (**C**) NF-κB activity in LLC-PK1 cells expressing WT KIM-1 or KIM-1$^{\Delta mucin}$ plus NF-κB–responsive promotor driving luciferase (normalized to *Renilla* luciferase driven by a constitutive promotor) (n = 4). $^{**}P < 0.0001$; $^{*}P < 0.01$. (**D** and **E**) Representative immunoprecipitation analysis of KIM-1 phosphorylation and interaction with p85 from 4 experiments. (**D**) LLC-PK1 cell lysates from WT and KIM-1$^{\Delta mucin}$–expressing cells were immunoprecipitated with an Ab against phosphorylated tyrosine residues and probed for KIM-1 by immunoblotting. (**E**) FLAG-tagged KIM-1 or KIM-1$^{\Delta mucin}$ was immunoprecipitated from lysates with anti-FLAG Abs and probed for p85 or KIM-1 by immunoblotting. (**F**) Representative images of LLC-PK1 cells expressing WT or KIM-1$^{\Delta mucin}$ incubated with apoptotic cells. Cells were stained for KIM-1 (green), p85 (red), and apoptotic cell proteins (blue). Scale bar: 10 μm. (**G**) Confocal z plane of WT KIM-1 cells stained as in **E** and imaged in a z series. N, LLC-PK1 cell nucleus. (**H**) 3D reconstruction of z series from **G** of KIM-1/p85 colocalization at a phagocytic event (upper right and individual channels in lower panels). Images in **G** and **H** are representative of 3 experiments. Scale bar: 5 μm (**G** and **H**). (**I**) Immunoblot analysis of p–NF-κB in KIM-1 or KIM-1$^{\Delta mucin}$ primary PTCs treated with vehicle or the PI3K inhibitors wortmannin or LY294002 (immunoblots are representative of 3 experiments). Groups were compared by ANOVA followed by Bonferroni's post-hoc analysis.

taining autoclaved glass coverslips. The epithelial cells were used in experiments between days 5 and 7 of culture.

Primary culture of BMMs

BMMs were generated using established methods. Briefly, BM cells were collected from WT B57CL/6 mice by flushing femurs and tibiae with RPMI 1640 containing 5% FCS, and erythrocytes were lysed. The cells were resuspended with macrophage culture medium (25% L929-conditioned medium in 10%FBS DMEM), passed through 40-μm meshes, and plated. The cells were kept in macrophage medium for 7 days and then used for experiments.

Plasmids, transfection, and lentiviral transduction

WT *KIM-1* and *KIM-1$^{\Delta mucin}$* sequences were derived using cDNA isolated from post-ischemic kidney tissue by PCR using flanking primers. PCR products were then inserted into pcDNA3 by restriction enzyme digestion (Invitrogen). WT *KIM-1* and *KIM-1$^{\Delta mucin}$* sequences were subcloned into the pCDH lentivector by restriction enzyme digestion (System Biosciences). Lentiviral particles were generated by transfecting LentiX 293T cells (Invitrogen) with pCDH, pCDH-WT *KIM-1* or pCDH-*KIM-1$^{\Delta mucin}$* cells at a 6:3:1:1 ratio with the packaging constructs pMDLg/pRRE, pRSV-REV, and VSVG, respectively (gift of Didier Trono, Addgene). All transfections were carried out using Lipofectamine 2000 (Invitrogen) following the manufacturer's protocol. Medium containing lentiviral particles was collected 48 and 72 hours after transfection. For lentiviral transduction, LLC-PK1 cells were plated at approximately 50% confluence and incubated with medium containing lentiviral particles and polybrene infection reagent at a 1:1,000 dilution (EMD Millipore). FLAG-tagged KIM-1 constructs were generated by PCR cloning. Briefly, the WT KIM-1 or KIM-1$^{\Delta mucin}$ sequence was amplified from the pcDNA vectors described above using the following primers: forward, 5′-GATTCCGAATTCACCATGAATCAGATTCAAGTCTTCATTTCAGGC-3′; reverse, 5′-GCTGCTCTCGAGCTACTTGTCATCGTCGTCCTTGTAGTCAGGTCTATCTTCAACAATGTAGATGTTGTC-3′. The resulting sequence was cloned into a pLVX-IRES-tdTomato vector (Clontech) using *EcoR1* and *Xho1* sites.

Cell culture and treatment

The LLC-PK1 (ATCC) cells or the primary cultured PTCs were incubated in serum-free DMEM for 24 hours and treated with either LPS (5 mg/ml) or TNF-α (10 ng/ml), with or without pre-feeding with apoptotic Jurkat cells (T lymphocytes; ATCC) for 2 hours. After 24 hours, the epithelial cells were washed 3 times with DMEM and incubated with fresh medium for an additional 24 hours. The conditioned medium was then collected and added to serum-starved BMMs or RAW264.7 monocytes/macrophages (ATCC) for another 24-hour treatment. LentiX 293T cells (Invitrogen) were grown in DMEM with 10% FBS.

DNA microarray analysis

RNA preparation for hybridization with DNA microarrays. The human prostate cancer cell line PC3 (ATCC) was transiently transduced with adenovirus expressing LacZ or hKIM-1 in triplicate. Total RNA was isolated using TRIzol solution (RNeasy Plus Mini Kit; QIAGEN). Total RNA (7 μg) was used for amplification. The amplified product was labeled with biotin. Briefly, double-stranded cDNA was synthesized using the SuperScript Choice System (Gibco BRL; Life Technologies) and a T7-(dT)-24 primer (Genset Oligos, Sigma-Aldrich). The cDNA was purified by phenol-chloroform-isoamyl alcohol extraction with Phase Lock Gel (5 Prime 3 Prime Inc.) and concentrated by ethanol precipitation. In vitro transcription was performed to produce biotin-labeled cRNA using a BioArray HighYield RNA Transcript Labeling Kit (Affymetrix) according to the manufacturer's instructions. cRNA was linearly amplified with T7 polymerase. The biotinylated RNA was cleaned with an RNeasy Mini Kit (QIAGEN). The resulting cRNA was probed using the CodeLink microarray (CodeLink Human Whole Genome Bioarray 300026.6; Amersham, GE Healthcare). The gene names and accession numbers are from the original CodeLink file. Labeled cRNA (20 μg) was fragmented, and the hybridization mixture was incubated at 99°C for 5 minutes, followed by incubation at 45°C for 5 minutes. The hybridization was then carried out at 45°C for 16 to 18 hours. After being washed, the array was stained with streptavidin-phycoerythrin (Molecular Probes), amplified by biotinylated antistreptavidin (Vector Laboratories), and then scanned on an HP Gene Array scanner. The intensity for each feature of the array was captured with Affymetrix GeneChip Software, according to the standard Affymetrix procedure, by performing typical scaling (with a target intensity of 100) and normalization for all probesets. Statistical analysis was performed using JMP (SAS Institute Inc.) and S-Plus (NCSS Statistical Software) software. Microarray raw data files are available in the European Bioinformatics Institute (EBI) ArrayExpress database (accession number E-MTAB-3225).

Quality control of samples. Total RNA collected from cells was subjected to a 1% agarose gel to assess the quality of RNA prior to in vitro transcription (IVT) preparation. In addition, each probe array contained several prokaryotic genes (e.g., *bioB*, *bioC*, and *bioD* are genes of the biotin synthesis pathway from the *E. coli* bacterium; *Cre* is the recombinase gene from the P1 bacteriophage), which served as hybridization controls. In addition, expression levels of 3′ to 5′ for both β-actin and GAPDH were evaluated, and, according to the manufacturer's instructions, the 3′ to 5′ ratio should be less than 3. Data failing to meet this criterion were excluded from analysis.

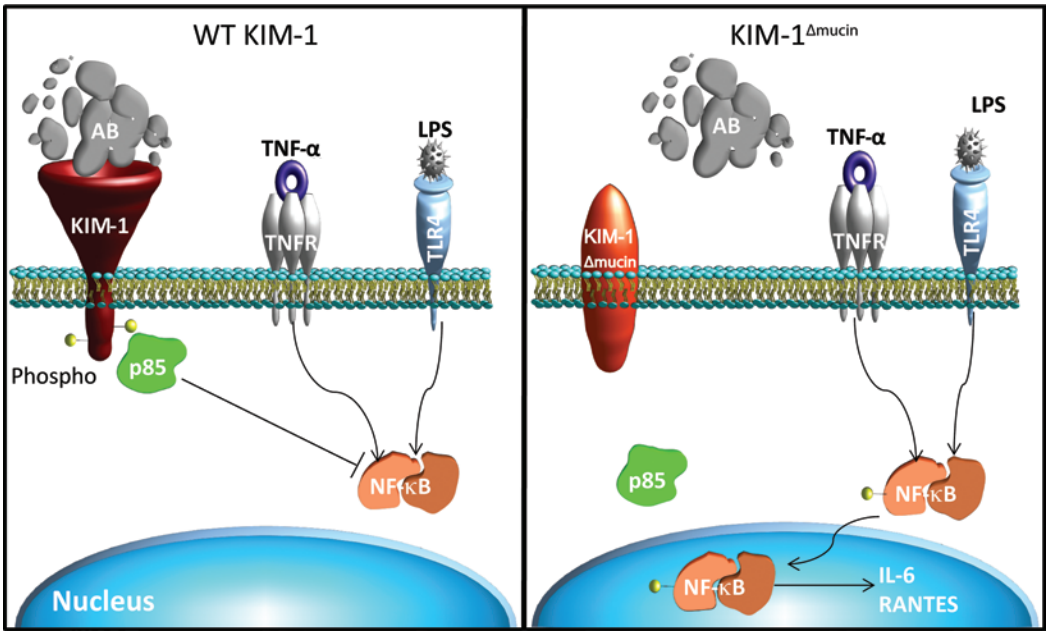

Figure 10. Proposed model of KIM-1 regulation of NF-κB. WT KIM-1 binding to apoptotic cells triggers KIM-1 phosphorylation and recruitment of p85, which then blocks the phosphorylation and activation of NF-κB. In cells expressing KIM-1$^{\Delta mucin}$, KIM-1$^{\Delta mucin}$ does not bind apoptotic cells and has reduced phosphorylation. This leads to reduced recruitment of p85 and greater phosphorylation and activation of NF-κB. AB, apoptotic body; Phospho, phosphorylation.

IPA. The genes identified by microarray analysis to be significantly up- or downregulated by human KIM-1 were further analyzed using IPA Core Analysis (QIAGEN) to generate interaction networks. The top 2 networks were merged to create the network shown in Figure 8. The connection between p85 and NF-κB was highlighted in red. The connection between KIM-1 (HAVCR1) and p85 was added based on interactions described in the literature (16). The molecules labeled in gray and KIM-1/HAVCR1 were from the microarray data, and the white and red molecules were included on the basis of IPA. Some molecules were removed from the network map in Figure 8 for clarity. The full list of genes used to generate the network can be found in Supplemental Tables 1 and 2.

Western blot analysis

Cells or kidney tissues were lysed, and lysates were prepared as previously described (50). Membranes were incubated with 1 or more of the following primary Abs: mouse anti–human KIM-1 and rabbit anti–mouse KIM-1 (1:200; Bonventre laboratory; R9, ref. 12); rabbit anti-p85 (1:1,000, ABS233; EMD Millipore); and mouse anti–p–NF-κB (1:1,000, 3633L; Cell Signaling Technology). HRP-conjugated secondary Abs were applied, and enhanced chemiluminescence (Amersham Biosciences, GE Healthcare) was used to detect proteins. Anti–β-actin Ab (1:5,000, A5441; Sigma-Aldrich) was used as a loading control on stripped membranes.

Immunoprecipitation

HEK-293 cells were transfected with empty vector, FLAG-tagged WT KIM-1, or FLAG-tagged KIM-1$^{\Delta mucin}$ using Lipofectamine 2000 according to the manufacturer's instructions and treated as described. Cells were lysed in a modified RIPA buffer, and 500 μg protein lysate was used for immunoprecipitation or coimmunoprecipitation analysis as described previously (51). Briefly, lysate was diluted to a final concentration of 500 μg/500 μl in detergent-free modified RIPA buffer. Lysate was precleared with 20 μl protein A/G/L beads in a 50% slurry for 1 hour at 4°C (BioVision). Lysate was then incubated with 0.5 μg chicken anti-FLAG Ab overnight at 4°C (ET-DY100; Aves Labs Inc.) for precipitation of FLAG-tagged proteins or with antiphosphotyrosine Ab (9411S; Cell Signaling Technology) for precipitation of tyrosine-phosphorylated proteins. Abs were precipitated with 20 μl protein A/G/L beads, and the resulting precipitate was washed 3 times with PBS and once with PBS plus an additional 500 mM NaCl. The beads were then resuspended in Western sample buffer containing DTT and boiled for 10 minutes. Precipitates were analyzed by immunoblotting.

Measurement of KIM-1, IL-6, and RANTES concentration using microbead-based ELISA

Cell lysates were prepared as described above, and total protein content was quantified using the Lowry method (reagents were purchased from Bio-Rad). KIM-1 concentration in the cell lysate was measured using Luminex xMAP Technology. In brief, cell lysate samples were incubated with approximately 6,000 anti-mouse KIM-1–coupled beads for 1 hour. Biotinylated detection Abs were applied, and quantification was achieved by incubating samples with streptavidin coupled with picoerythrin (Invitrogen), which is excited at 532 nm. The signal from this fluorochrome was directly proportional to the amount of antigen bound at the microbead surface that was detected using the Bio-Plex system (Bio-Rad). RANTES and IL-6 microbead–based assays were developed and validated in the laboratory and performed as described above for KIM-1. The following Abs used were purchased from R&D Systems: IL-6: capture Ab (MAB 406), detection Ab (BAF406), and IL-6 standard (406-ML-200); RANTES: capture Ab (MAB4781), detection Ab (BAF478), and RANTES standard (478-MR-025); KIM-1: capture Ab (MAB1817), detection Ab (BAF1817), and standard (1817-050). Data were interpreted using a 13-point standard 5-parameter logistic regression model. All samples were analyzed in triplicate, and the intra-assay variability was less than 15%.

Quantitation of mRNA by real-time quantitative RT-PCR

Total RNA was isolated from either the kidneys or the cultured tubule cells and macrophages using TRIzol reagent according to the stan-

dard protocol. Total RNA (5 μg) was reverse transcribed using the M-MLV Reverse Transcriptase Kit and Oligo dT Primers (both from Promega). Real-time PCR was performed using the SYBR Green gene expression assays (Bio-Rad) for detection of mRNA expression levels of *KIM-1*, *Tlr1–4*, *Tlr7*, *Tlr9*, *Ccl2*, *Il6*, *Tnf*, and *Il1b*. *Gapdh* was used as an internal control.

Immunofluorescence staining

Immunofluorescence staining of the kidney was performed on paraffin or frozen sections as previously described (31). The primary Abs included rabbit anti–KIM-1 (1:200, R9, Bonventre laboratory; ref. 12); goat anti-TLR4 (1:400, SC-12511; Santa Cruz Biotechnology Inc.); rat anti-F4/80 (1:100, HB-198; ATCC Hybridoma) (12); rabbit anti-CD3 (1:500, SP7; Abcam); FITC-coupled mouse anti-Ly6G (1:200, RB6-8C5; Sigma-Aldrich); and rabbit anti-laminin (1:500, ab11575; Abcam). The slides were then exposed to FITC- or Cy3-labeled secondary Abs. The staining was examined using fluorescence microscopes (Nikon TE 1000 and Nikon C1 confocal). The number of infiltrating cells was measured by counting 5 high-powered fields from the outer medulla in each kidney examined. Immunofluorescence staining of KIM-1, TLR4, and Ki67 (VP-RMo4; Vector Laboratories) was also performed on primary tubular cells as previously described (31). LLC-PK1 cells expressing KIM-1 or KIM-1$^{\Delta mucin}$ were stained with anti–KIM-1 (1:200, R9; Bonventre laboratory; ref. 12) and anti-p85 (1:1,000, ABS233; EMD Millipore). In some cases, BMMs were incubated with BrdU (100 μg/ml) and added to the culture medium 2 hours before harvesting.

Cell death assay

Apoptosis in kidney tissues and primary cultured PTCs was detected on paraffin sections by the in situ TUNEL method following the standard protocol (Roche). Cell toxicity was determined by lactic dehydrogenase (LDH) release assay according to standard methods.

Luciferase assay for NF-κB activity

NF-κB activity was measured using an NF-κB luciferase reporter. pNF-κB-Luc and *Renilla* luciferase vectors were purchased from Stratagene. Stable cell lines were generated by cotransfection of pNF-κB–Luc/*Renilla* with pcDNA, KIM-1, or KIM-1$^{\Delta mucin}$ into LLC-PK1 cells. Cells were selected by incubation with G418. Stable cell lines were plated in a 96-well plate and treated as indicated in Figure 9C. Following treatment, luciferase activity was measured with the Promega Dual Luciferase Reporter Assay System according to the manufacturer's instructions. Luciferase activity was standardized by the ratio of NF-κB–dependent firefly luciferase to the internal control *Renilla* luciferase.

ELISA

TNF-α was measured in the supernatant of cultured cells using ELISA kits (DuoSet ELISA, DY410; R&D Systems) according to the manufacturer's instructions. Cytokine protein levels were corrected for the total amount of cell lysis protein, and the results were expressed as pg/ml. The lower detection limit was 50 pg/ml.

Statistics

Results are expressed as the mean ± SD. ANOVA was used to compare data among groups. A 2-tailed Student's *t* test was used to determine significant differences between 2 groups. ANOVA followed by Bonferroni's post-hoc analysis was used to determine significant differences between groups of 3 or more. Correlations were assessed according to Pearson's correlation analysis. A *P* value of less than 0.05 was considered significant.

Study approval

All animal experiments were performed in accordance with the animal care and use protocol approved by the IACUC of Harvard Medical School.

Acknowledgments

This work was supported by NIH grants DK39773 and DK72381 (to J.V. Bonventre); DK088418 (to C.R. Brooks); and National Natural Science Foundation of China Grant 81270777 (to L. Yang). We would like to thank J. Wilflingseder for her assistance in analyzing the microarray data and in generating the microarray heatmap.

Address correspondence to: Joseph V. Bonventre or Craig R. Brooks, Harvard Institutes of Medicine, Room 576, 4 Blackfan Circle, Boston, Massachusetts 02115, USA. Phone: 617.732.5960; E-mail: joseph_bonventre@hms.harvard.edu (J.V. Bonventre); crbrooks@partners.org (C.R. Brooks). Or to: Li Yang, Peking University First Hospital, 8 Xishiku St., Renal Division, Xicheng Distric, Beijing, China 100034. E-mail: li.yang@bjmu.edu.cn.

1. Lameire N, Van Biesen W, Vanholder R. The changing epidemiology of acute renal failure. *Nat Clin Pract Nephrol*. 2006;2(7):364–377.
2. Uchino S, et al. Acute renal failure in critically ill patients: a multinational, multicenter study. *JAMA*. 2005;294(7):813–818.
3. Hsu CY, Chertow GM, McCulloch CE, Fan D, Ordonez JD, Go AS. Nonrecovery of kidney function and death after acute on chronic renal failure. *Clin J Am Soc Nephrol*. 2009;4(5):891–898.
4. Ishani A, et al. Acute kidney injury increases risk of ESRD among elderly. *J Am Soc Nephrol*. 2009;20(1):223–228.
5. Coca SG, Yusuf B, Shlipak MG, Garg AX, Parikh CR. Long-term risk of mortality and other adverse outcomes after acute kidney injury: a systematic review and meta-analysis. *Am J Kidney Dis*. 2009;53(6):961–973.
6. Bonventre JV. Dedifferentiation and proliferation of surviving epithelial cells in acute renal failure. *J Am Soc Nephrol*. 2003;14(suppl 1):S55–S61.
7. Humphreys BD, Bonventre JV. Mesenchymal stem cells in acute kidney injury. *Annu Rev Med*. 2008;59:311–325.
8. Humphreys BD, Czerniak S, Dirocco DP, Hasnain W, Cheema R, Bonventre JV. Repair of injured proximal tubule does not involve specialized progenitors. *Proc Natl Acad Sci U S A*. 2011;108(22):9226–9231.
9. Yang L, Besschetnova TY, Brooks CR, Shah JV, Bonventre JV. Epithelial cell cycle arrest in G2/M mediates kidney fibrosis after injury. *Nat Med*. 2010;16(5):535–543.
10. Grgic I, et al. Targeted proximal tubule injury triggers interstitial fibrosis and glomerulosclerosis. *Kidney Int*. 2012;82(2):172–183.
11. Bonventre JV, Zuk A. Ischemic acute renal failure: an inflammatory disease? *Kidney Int*. 2004;66(2):480–485.
12. Ichimura T, Hung CC, Yang SA, Stevens JL, Bonventre JV. Kidney injury molecule-1: a tissue and urinary biomarker for nephrotoxicant-induced renal injury. *Am J Physiol Renal Physiol*. 2004;286(3):F552–F563.
13. Bonventre JV. Kidney injury molecule-1 (KIM-1): a urinary biomarker and much more. *Nephrol Dial Transplant*. 2009;24(11):3265–3268.
14. Ichimura T, Asseldonk EJ, Humphreys BD, Gunaratnam L, Duffield JS, Bonventre JV. Kidney injury molecule-1 is a phosphatidylserine receptor that confers a phagocytic phenotype on epithelial cells. *J Clin Invest*. 2008;118(5):1657–1668.
15. Humphreys BD, et al. Chronic epithelial kidney injury molecule-1 expression causes murine kid-

ney fibrosis. *J Clin Invest*. 2013;123(9):4023–4035.
16. de Souza AJ, Oak JS, Jordanhazy R, DeKruyff RH, Fruman DA, Kane LP. T cell Ig and mucin domain-1-mediated T cell activation requires recruitment and activation of phosphoinositide 3-kinase. *J Immunol*. 2008;180(10):6518–6526.
17. Xiao S, et al. Defect in regulatory B-cell function and development of systemic autoimmunity in T-cell Ig mucin 1 (Tim-1) mucin domain-mutant mice. *Proc Natl Acad Sci U S A*. 2012;109(30):12105–12110.
18. Rennert PD. Novel roles for TIM-1 in immunity and infection. *Immunol Lett*. 2011;141(1):28–35.
19. Xiao S, et al. Tim-1 stimulation of dendritic cells regulates the balance between effector and regulatory T cells. *Eur J Immunol*. 2011;41(6):1539–1549.
20. Erwig LP, Henson PM. Immunological consequences of apoptotic cell phagocytosis. *Am J Pathol*. 2007;171(1):2–8.
21. Erwig LP, Henson PM. Clearance of apoptotic cells by phagocytes. *Cell Death Differ*. 2008;15(2):243–250.
22. Hart SP, Dransfield I, Rossi AG. Phagocytosis of apoptotic cells. *Methods*. 2008;44(3):280–285.
23. Li L, et al. NKT cell activation mediates neutrophil IFN-gamma production and renal ischemia-reperfusion injury. *J Immunol*. 2007;178(9):5899–5911.
24. Lin SL, Kisseleva T, Brenner DA, Duffield JS. Pericytes and perivascular fibroblasts are the primary source of collagen-producing cells in obstructive fibrosis of the kidney. *Am J Pathol*. 2008;173(6):1617–1627.
25. Pollard JW. Trophic macrophages in development and disease. *Nat Rev Immunol*. 2009;9(4):259–270.
26. Zhang MZ, et al. CSF-1 signaling mediates recovery from acute kidney injury. *J Clin Invest*. 2012;122(12):4519–4532.
27. Bonventre JV, Yang L. Cellular pathophysiology of ischemic acute kidney injury. *J Clin Invest*. 2011;121(11):4210–4221.
28. Yang L, Humphreys BD, Bonventre JV. Pathophysiology of acute kidney injury to chronic kidney disease: maladaptive repair. *Contrib Nephrol*. 2011;174:149–155.
29. Bousquet C, et al. Direct binding of p85 to sst2 somatostatin receptor reveals a novel mechanism for inhibiting PI3K pathway. *EMBO J*. 2006;25(17):3943–3954.
30. Cuevas BD, et al. Tyrosine phosphorylation of p85 relieves its inhibitory activity on phosphatidylinositol 3-kinase. *J Biol Chem*. 2001;276(29):27455–27461.
31. Ichimura T, et al. Kidney injury molecule-1 (KIM-1), a putative epithelial cell adhesion molecule containing a novel immunoglobulin domain, is up-regulated in renal cells after injury. *J Biol Chem*. 1998;273(7):4135–4142.
32. Jang HR, Rabb H. The innate immune response in ischemic acute kidney injury. *Clin Immunol*. 2009;130(1):41–50.
33. Wolfs TG, et al. In vivo expression of Toll-like receptor 2 and 4 by renal epithelial cells: IFN-γ and TNF-α mediated up-regulation during inflammation. *J Immunol*. 2002;168(3):1286–1293.
34. Kim BS, et al. Ischemia-reperfusion injury activates innate immunity in rat kidneys. *Transplantation*. 2005;79(10):1370–1377.
35. Wu H, et al. TLR4 activation mediates kidney ischemia/reperfusion injury. *J Clin Invest*. 2007;117(10):2847–2859.
36. Pulskens WP, et al. Toll-like receptor-4 coordinates the innate immune response of the kidney to renal ischemia/reperfusion injury. *PLoS One*. 2008;3(10):e3596.
37. Aderem A, Ulevitch RJ. Toll-like receptors in the induction of the innate immune response. *Nature*. 2000;406(6797):782–787.
38. Savill J, Dransfield I, Gregory C, Haslett C. A blast from the past: clearance of apoptotic cells regulates immune responses. *Nat Rev Immunol*. 2002;2(12):965–975.
39. Barker RN, Erwig LP, Hill KS, Devine A, Pearce WP, Rees AJ. Antigen presentation by macrophages is enhanced by the uptake of necrotic, but not apoptotic, cells. *Clin Exp Immunol*. 2002;127(2):220–225.
40. Fadok VA, Bratton DL, Guthrie L, Henson PM. Differential effects of apoptotic versus lysed cells on macrophage production of cytokines: role of proteases. *J Immunol*. 2001;166(11):6847–6854.
41. Zingg JM, Ricciarelli R, Azzi A. Scavenger receptors and modified lipoproteins: fatal attractions? *IUBMB Life*. 2000;49(5):397–403.
42. Wong SH, Barlow JL, Nabarro S, Fallon PG, McKenzie AN. Tim-1 is induced on germinal centre B cells through B-cell receptor signalling but is not essential for the germinal centre response. *Immunology*. 2010;131(1):77–88.
43. Ding Q, et al. Regulatory B cells are identified by expression of TIM-1 and can be induced through TIM-1 ligation to promote tolerance in mice. *J Clin Invest*. 2011;121(9):3645–3656.
44. Jang HR, Gandolfo MT, Ko GJ, Satpute SR, Racusen L, Rabb H. B cells limit repair after ischemic acute kidney injury. *J Am Soc Nephrol*. 2010;21(4):654–665.
45. Nozaki Y, Nikolic-Paterson DJ, Yagita H, Akiba H, Holdsworth SR, Kitching AR. Tim-1 promotes cisplatin nephrotoxicity. *Am J Physiol Renal Physiol*. 2011;301(5):F1098–F1104.
46. Rong S, et al. The TIM-1:TIM-4 pathway enhances renal ischemia-reperfusion injury. *J Am Soc Nephrol*. 2011;22(3):484–495.
47. Ichimura T, Brooks CR, Bonventre JV. Kim-1/Tim-1 and immune cells: shifting sands. *Kidney Int*. 2012;81(9):809–811.
48. Park KM, Byun JY, Kramers C, Kim JI, Huang PL, Bonventre JV. Inducible nitric oxide synthase is an important contributor to prolonged protective effects of ischemic preconditioning in the mouse kidney. *J Biol Chem*. 2003;278(29):27256–27266.
49. Zahedi K, et al. Stathmin-deficient mice develop fibrosis and show delayed recovery from ischemic-reperfusion injury. *Am J Physiol Renal Physiol*. 2006;290(6):F1559–F1567.
50. Hung CC, Ichimura T, Stevens JL, Bonventre JV. Protection of renal Epithelial cells against oxidative injury by endoplasmic reticulum stress preconditioning is mediated by ERK1/2 activation. *J Biol Chem*. 2003;278(31):29317–29326.
51. Hsu SI, Yang CM, Sim KG, Hentschel DM, O'Leary E, Bonventre JV. TRIP-Br: a novel family of PHD zinc finger- and bromodomain-interacting proteins that regulate the transcriptional activity of E2F-1/DP-1. *EMBO J*. 2001;20(9):2273–2285.